Available online at www.sciencedirect.com
ScienceDirect
Journal of Computational Physics 227 (2007) 574–601
JOURNAL OF COMPUTATIONAL PHYSICS
www.elsevier.com/locate/jcp

On a well-balanced high-order finite volume scheme for shallow water equations with topography and dry areas ☆

José M. Gallardo *, Carlos Parés, Manuel Castro

Department of Mathematical Analysis, University of Málaga, Campus Teatinos s/n, 29080 Málaga, Spain

Received 8 March 2007; received in revised form 3 August 2007; accepted 7 August 2007
Available online 23 August 2007

Abstract

We present a finite volume scheme for solving shallow water equations with source term due to the bottom topography. The scheme has the following properties: it is high-order accurate in smooth wet regions, it correctly solves situations where dry areas are present, and it is well-balanced. The scheme is developed within a general nonconservative framework, and it is based on hyperbolic reconstructions of states. The treatment of wet/dry fronts is carried out by solving specific nonlinear Riemann problems at the corresponding intercells.

MSC: 65M06; 35L65; 76M12; 76B15

Keywords: Hyperbolic systems; Nonconservative products; High-order schemes; Well-balanced schemes; Roe methods; Shallow water systems; Wet/dry fronts

1. Introduction

Shallow water equations are widely used in ocean and hydraulic engineering to model flows in rivers, reservoirs or coastal areas, among others applications. In the form considered in this paper, they constitute a hyperbolic system of conservation laws with a source term due to the bottom topography.

In recent years, there has been increasing interest in the design of numerical schemes with good properties for shallow water equations (see, e.g. [8,13,26,35–37], and the references therein). It is a challenge to obtain schemes that compute solutions with high-order accuracy (both in space and time) in the regions where they are smooth, while at the same time shock discontinuities are properly captured. However, when a source term is present the schemes must also satisfy a balance between the flux and the source terms, in order to properly

☆ Research partially supported by the Spanish Government Research Project MTM06-08075.
* Corresponding author. Tel.: +34 952 131 898; fax: +34 952 131 894.
E-mail addresses: gallardo@anamat.cie.uma.es (J.M. Gallardo), pares@anamat.cie.uma.es (C. Parés), castro@anamat.cie.uma.es (M. Castro).

0021-9991/$ - see front matter
doi:10.1016/j.jcp.2007.08.007

compute stationary or almost stationary solutions. This property is known as *well-balancing*, and it is currently an active subject of research (see, e.g. [4,5,8,13,14,16,22,3,26,27,35–37]).

In [8], a high-order well-balanced finite volume scheme was developed within a general nonconservative framework. The scheme uses high-order reconstruction of states and it is based on the generalized Roe schemes introduced in [34], whose well-balance properties have been studied in [27]. In particular, it was successfully applied to shallow water equations with bottom topography, using fifth-order WENO reconstructions in space and a third-order TVD Runge–Kutta scheme to advance in time.

An important difficulty arising in the simulation of free surface flows is the appearance of dry areas, due to the initial conditions or as a result of the fluid motion. Examples are numerous: flood waves, dambreaks, breaking of waves on beaches, etc. If no modifications are made, standard numerical schemes may fail in the presence of wet/dry situations, producing spurious results. Several methods can be found in the literature which overcome this problem: see [5,33] for a review.

When applied to shallow water equations, the Roe schemes introduced in [27] loose their well-balance properties in the presence of wet/dry transitions. Moreover, they may produce negative values of the thickness of the water layer in the proximities of the wet/dry front. In [10], a modification was proposed that partially overcomes this problem. Recently, a new technique for treating wet/dry fronts in the context of Roe schemes has been presented in [9]. It consists in replacing, at the intercells where a wet/dry transition has been detected, the corresponding linear Riemann problem by an adequate nonlinear one.

The main idea in the present work is to properly combine the scheme developed in [8] with the treatment of wet/dry fronts introduced in [9]. This is by no means a trivial task, as many difficulties appear. In particular, the numerical fluxes must be modified according to the kind of wet/dry transition found. Moreover, the variables to be reconstructed have to be properly chosen in order to maintain the well-balance property and, at the same time, to preserve the positivity of the water height.

Specifically, the LHHR method introduced in [24] has been considered; we prove that this reconstruction method is indeed positivity-preserving. The resulting scheme is third-order accurate on smooth wet regions and first-order accurate near shocks and wet/dry transitions. Moreover, as a consequence of the positivity of the reconstruction operator and the results in [9], the positivity of the water height is maintained (though in some cases a reduction of the CFL number is necessary).

A two-dimensional extension of the scheme, based on the bi-hyperbolic method proposed in [29], has also been carried out.

The paper is structured as follows. In Section 2 the precise form of the shallow water equations to be solved is stated in the one-dimensional case, and some known definitions and results about nonconservative hyperbolic systems and generalized Roe schemes are given. The construction of the scheme developed in [8] is summarized in Section 3, and an alternative form of the scheme in the case of shallow water equations with topography is also provided. Section 4 is devoted to reviewing the technique introduced in [9] for the treatment of wet/dry fronts. The core of the paper are Sections 5 and 6, where a high-order well-balanced scheme capable of dealing with wet/dry situations is constructed. In Section 7 a two-dimensional extension of the scheme is also introduced. A number of numerical experiments are performed in Section 8 in order to test the properties of the numerical scheme, both in the one- and two-dimensional cases. The paper finishes with some concluding remarks and an Appendix, where the positivity of the LHHR method is proved.

2. Preliminaries

We consider the one-dimensional shallow water system given by

$$\begin{cases} \frac{\partial h}{\partial t} + \frac{\partial q}{\partial x} = 0, \\ \frac{\partial q}{\partial t} + \frac{\partial}{\partial x}\left(\frac{q^2}{h} + \frac{g}{2}h^2\right) = gh\frac{dH}{dx}, \end{cases} \tag{2.1}$$

which are the equations governing the flow of a shallow layer of fluid through a straight channel with constant rectangular cross-section. The variable x refers to the axis of the channel and t is time; $h(x, t)$ and $q(x, t)$ represent the thickness and the discharge, respectively; g is the gravity constant; finally, $H(x)$ is the depth function

measured from a fixed level of reference. The fluid is supposed to be homogeneous and inviscid. The terms modelling bottom friction or wind effects are not considered here for simplicity.

Addition of the equation [21]

$$\frac{\partial H}{\partial t} = 0$$

to (2.1) allows us to write the system in *nonconservative* form:

$$W_t + \mathcal{A}(W)W_x = 0, \qquad x \in \mathbb{R}, \quad t > 0. \tag{2.2}$$

The state variable is given by

$$W = \begin{bmatrix} h \\ q \\ H \end{bmatrix}$$

and the matrix $\mathcal{A}(W)$ is defined as

$$\mathcal{A}(W) = \begin{bmatrix} 0 & 1 & 0 \\ -u^2 + c^2 & 2u & -c^2 \\ 0 & 0 & 0 \end{bmatrix},$$

where $u = q/h$ is the averaged velocity and $c = \sqrt{gh}$.

As long as dry zones do not occur, the variable W takes its values in the open convex set

$$\Omega = \{[h, q, H]^{\mathrm{T}} : h > 0, q \in \mathbb{R}, H \in \mathbb{R}\}.$$

Although in this article we will be eventually interested in the case where W belongs to $\overline{\Omega} = \Omega \cup \{[0, 0, H]^{\mathrm{T}} : H \in \mathbb{R}\}$, thus allowing the presence of dry zones, we will assume along this section that the condition $h > 0$ holds. The treatment of wet/dry zones will be analyzed in Section 4.

The eigenvalues of the matrix $\mathcal{A}(W)$ are

$$\lambda_1 = u - c, \quad \lambda_2 = u + c, \quad \lambda_3 = 0.$$

If $h > 0$ and $\lambda_i \neq 0$, $i = 1, 2$, the system (2.2) is strictly hyperbolic and a complete set of eigenvectors is given by

$$R_i(W) = \begin{bmatrix} 1 \\ \lambda_i \\ 0 \end{bmatrix}, \quad i = 1, 2; \quad R_3(W) = \begin{bmatrix} 1 \\ 0 \\ 1 - Fr^2 \end{bmatrix},$$

where $Fr = u/c$ is the Froude number.

Notice that when (2.2) is strictly hyperbolic, the characteristic fields R_1 and R_2 are genuinely nonlinear, while R_3 is linearly degenerate. The integral curves of the third characteristic field are given by

$$q = q_0, \quad h + \frac{q^2}{2gh^2} - H = C, \tag{2.3}$$

where q_0 and C are arbitrary constants. In the particular case $q = 0$, we obtain the water at rest states:

$$q = 0, \quad h - H = C. \tag{2.4}$$

The nonconservative product $\mathcal{A}(W)W_x$ does not make sense, in general, within the framework of the theory of distributions. More precisely, the term ghH_x does not make sense if both h and H have discontinuities at the same points. However, following the theory developed by Dal Maso et al. [11], it is possible to give a sense to the nonconservative product as a Borel measure. We refer to [11] for technical details.

Many of the usual numerical schemes designed for systems of conservation laws can be adapted to the discretization of the nonconservative system (2.2). This is the case of Roe schemes, whose general definition is based on the concept of *Roe linearization* introduced in [34]: the interested reader is referred to that article

and to [27] for a complete description of generalized Roe schemes. Here, we restrict ourselves to the particular case in which the Roe matrices are given, for arbitrary states $W_0, W_1 \in \Omega$, by

$$\hat{\mathcal{A}}(W_0, W_1) = \begin{bmatrix} 0 & 1 & 0 \\ -\hat{u}^2 + \hat{c}^2 & 2\hat{u} & -\hat{c}^2 \\ 0 & 0 & 0 \end{bmatrix},$$

where

$$\hat{u} = \frac{\sqrt{h_0}u_0 + \sqrt{h_1}u_1}{\sqrt{h_0} + \sqrt{h_1}}, \quad \hat{c} = \sqrt{g\frac{h_0 + h_1}{2}} \tag{2.5}$$

are the usual Roe states [28].

In order to discretize the system, the space domain is divided into computing cells $I_i = [x_{i-1/2}, x_{i+1/2}]$. For the sake of simplicity, it is assumed that the cells have constant size Δx and that $x_{i+1/2} = i\Delta x$; thus, $x_i = (i - 1/2)\Delta x$ is the center of the cell I_i. Let Δt be the time step and $t^n = n\Delta t$. Denote by $W_i^n = [h_i^n, q_i^n, H_i^n]^{\mathrm{T}}$ the approximation of the cell averages on I_i of the exact solution, at time t^n:

$$W_i^n \cong \frac{1}{\Delta x}\int_{x_{i-1/2}}^{x_{i+1/2}} W(x, t^n)\,\mathrm{d}t.$$

Given the states W_i^n and W_{i+1}^n, the intermediate Roe matrix is defined as

$$\mathcal{A}_{i+1/2} = \hat{\mathcal{A}}(W_i^n, W_{i+1}^n).$$

As usual, if $\lambda_1^{i+1/2} < \lambda_2^{i+1/2} < \lambda_3^{i+1/2}$ are the eigenvalues of $\mathcal{A}_{i+1/2}$, we define

$$\mathcal{A}_{i+1/2}^{\pm} = \mathcal{K}_{i+1/2}\mathcal{L}_{i+1/2}^{\pm}\mathcal{K}_{i+1/2}^{-1},$$

where $\mathcal{L}_{i+1/2}^{\pm} = \mathrm{diag}\{\lambda_j^{i+1/2} : j = 1, 2, 3\}$ and $\mathcal{K}_{i+1/2}$ is a matrix whose columns are associated eigenvectors.

The numerical scheme can be written as follows:

$$W_i^{n+1} = W_i^n - \frac{\Delta t}{\Delta x}\left(\mathcal{A}_{i-1/2}^{+}(W_i^n - W_{i-1}^n) + \mathcal{A}_{i+1/2}^{-}(W_{i+1}^n - W_i^n)\right). \tag{2.6}$$

In practice, only the two first components in (2.6) will be taken into account, as they give the evolution of the variables h and q. The third component reduces to $H_i^{n+1} = H_i^n$, reflecting the fact that the depth function H is constant in time.

In what follows, we deduce an equivalent writing for (2.6) that will be of particular interest in Section 4. Define $U = [h, q]^{\mathrm{T}}$, so we denote $W = [U, H]^{\mathrm{T}}$. Using this notation, the system (2.1) can be interpreted as a conservation law with source term (or balance law):

$$\frac{\partial U}{\partial t} + \frac{\partial}{\partial x}F(U) = S(U)\frac{\mathrm{d}H}{\mathrm{d}x}. \tag{2.7}$$

The flux function and the source term are given, respectively, by

$$F(U) = \begin{bmatrix} q \\ \frac{q^2}{h} + \frac{g}{2}h^2 \end{bmatrix}, \quad S(U) = \begin{bmatrix} 0 \\ gh \end{bmatrix}.$$

Define $U_i^n = [h_i^n, q_i^n]^{\mathrm{T}}$ and consider the usual Roe matrix [28] defined as

$$A_{i+1/2} = \begin{bmatrix} 0 & 1 \\ -(u_{i+1/2}^n)^2 + (c_{i+1/2}^n)^2 & 2u_{i+1/2}^n \end{bmatrix},$$

where $u_{i+1/2}^n$ and $c_{i+1/2}^n$ are given by (2.5) using the states U_i^n and U_{i+1}^n. This matrix satisfies the so-called *Roe property*:

$$A_{i+1/2}(U_{i+1}^n - U_i^n) = F(U_{i+1}^n) - F(U_i^n).$$

Dropping the third component in (2.6) we can deduce, after some straightforward calculations, the following scheme:

$$U_i^{n+1} = U_i^n + \frac{\Delta t}{\Delta x}(F^+_{i-1/2} - F^-_{i+1/2}), \tag{2.8}$$

where the numerical fluxes are given by

$$\begin{aligned} F^-_{i+1/2} &= F(U_i^n) + P^-_{i+1/2}\big(A_{i+1/2}(U^n_{i+1} - U^n_i) - S_{i+1/2}\big),\\ F^+_{i+1/2} &= F(U^n_{i+1}) - P^+_{i+1/2}\big(A_{i+1/2}(U^n_{i+1} - U^n_i) - S_{i+1/2}\big). \end{aligned} \tag{2.9}$$

The numerical source term is defined as

$$S_{i+1/2} = \begin{bmatrix} 0 \\ (c^n_{i+1/2})^2(H(x_{i+1}) - H(x_i)) \end{bmatrix}.$$

The projection matrices $P^\pm_{i+1/2}$ are

$$P^\pm_{i+1/2} = \frac{1}{2}K_{i+1/2}(I \pm \operatorname{sgn}(\Lambda_{i+1/2}))K^{-1}_{i+1/2},$$

where $\operatorname{sgn}(\Lambda_{i+1/2}) = \operatorname{diag}\{\operatorname{sgn}(\lambda_j^{i+1/2}) : j = 1, 2\}$, being $\lambda_1^{i+1/2}$, $\lambda_2^{i+1/2}$ the eigenvalues of $A_{i+1/2}$ (which are the two first eigenvalues of $\mathcal{A}_{i+1/2}$) and $K_{i+1/2}$ a matrix whose columns are associated eigenvectors.

Remark 2.1. Substracting the first equation in (2.9) from the second one and using the Roe property, gives the equality

$$F^+_{i+1/2} - F^-_{i+1/2} = S_{i+1/2},$$

which implies an interface representation of the source term in (2.8).

Remark 2.2. The numerical scheme (2.8) is also equivalent to the Q-scheme of Roe upwinding the source term introduced in [4].

Concerning the stability requirements, we consider a CFL condition of the form

$$\max\left\{\left|\lambda_j^{i+1/2}\right| : 1 \leqslant j \leqslant 2,\ 0 \leqslant i \leqslant M\right\}\frac{\Delta t}{\Delta x} \leqslant \mu,$$

where $0 < \mu \leqslant 1$ and M is the number of cells into which the space domain is decomposed. Finally, the entropy-fix technique of Harten–Hyman [17] has also been applied.

As it is well-known, the presence of source or coupling terms in general systems of conservation laws can affect the quality of the numerical solution when steady or nearly steady state solutions are approximated. To handle such problems, the concept of *well-balanced* schemes has been considered by many authors (see, e.g. [4,5,14,16,22,3], etc.). In [27], a general definition of well-balancing for general nonconservative problems has been introduced.

In the context of shallow water equations (2.1), a scheme is *well-balanced with order* γ if it approximates the steady state solutions (2.3) with order γ, and it is *exactly well-balanced* if the steady state solutions are exactly computed. In [27] it is proved that the scheme (2.6) is well-balanced with order two for general stationary solutions of the form (2.3). Moreover, it solves exactly stationary solutions corresponding to water at rest, that is, it has the so-called C-property introduced and proved in [4].

3. High-order Roe schemes

The generalized Roe schemes introduced in the previous section are only first-order accurate. Recently, in [8] a high-order extension of the scheme (2.6) based on reconstructions of the state variable W was introduced. We give here a brief review about the construction of such extension. It will be assumed throughout this section that no dry zones are present.

First, we consider a *reconstruction operator* of order p, that is, an operator that assigns to a given sequence $\{W_i\}$ two new sequences, $\{W^-_{i+1/2}\}$ and $\{W^+_{i+1/2}\}$, such that

$$W^\pm_{i+1/2} = W(x_{i+1/2}) + \mathcal{O}(\Delta x^p),$$

whenever

$$W_i = \frac{1}{\Delta x}\int_{x_{i-1/2}}^{x_{i+1/2}} W(x)\,\mathrm{d}x$$

for some smooth function $W(x)$.

Let now $W_i(t) = [h^t_i, q^t_i, H^t_i]^{\mathrm{T}}$ be the cell average of a regular solution $W(x, t)$ of (2.2) on the cell I_i at a fixed time t:

$$W_i(t) = \frac{1}{\Delta x}\int_{x_{i-1/2}}^{x_{i+1/2}} W(x,t)\,\mathrm{d}x,$$

and denote by $W^\pm_{i+1/2}(t) = [h^{\pm,t}_{i+1/2}, q^{\pm,t}_{i+1/2}, H^{\pm,t}_{i+1/2}]^{\mathrm{T}}$ the corresponding reconstructions at the intercell $x_{i+1/2}$. We also introduce regular functions $\mathcal{R}^{-,t}_{i+1/2}(x)$ and $\mathcal{R}^{+,t}_{i+1/2}(x)$ defined, respectively, on $[x_i, x_{i+1/2}]$ and $[x_{i+1/2}, x_{i+1}]$, such that

$$\lim_{x\to x^-_{i+1/2}} \mathcal{R}^{-,t}_{i+1/2}(x) = W^-_{i+1/2}(t), \quad \lim_{x\to x^+_{i+1/2}} \mathcal{R}^{+,t}_{i+1/2}(x) = W^+_{i+1/2}(t).$$

Then, the following semidiscrete formulation of the high-order extension of the numerical scheme (2.6) is considered [8]:

$$\begin{aligned} W_i'(t) = &-\frac{1}{\Delta x}\Big(\mathcal{A}^+_{i-1/2}(W^+_{i-1/2}(t) - W^-_{i-1/2}(t)) + \mathcal{A}^-_{i+1/2}(W^+_{i+1/2}(t) - W^-_{i+1/2}(t)) \\ &+ \int_{x_{i-1/2}}^{x_i} \mathcal{A}(\mathcal{R}^{+,t}_{i-1/2}(x))\frac{\mathrm{d}}{\mathrm{d}x}\mathcal{R}^{+,t}_{i-1/2}(x)\,\mathrm{d}x + \int_{x_i}^{x_{i+1/2}} \mathcal{A}(\mathcal{R}^{-,t}_{i+1/2}(x))\frac{\mathrm{d}}{\mathrm{d}x}\mathcal{R}^{-,t}_{i+1/2}(x)\,\mathrm{d}x\Big), \end{aligned} \tag{3.1}$$

where $\mathcal{A}_{i+1/2}$ is the intermediate Roe matrix corresponding to the states $W^-_{i+1/2}(t)$ and $W^+_{i+1/2}(t)$.

Remark 3.1. As we stated in Section 2, the nonconservative product $\mathcal{A}(W)W_x$ is interpreted as a Borel measure. Roughly speaking, the two first terms in the right-hand side of (3.1) are related to the singular part of the measure, while the integral terms are associated to its regular part. Technical details can be found in [8].

If the balance-law formulation (2.7) is considered (as we will do in Section 6), (3.1) can be rewritten as follows:

$$U_i'(t) = \frac{1}{\Delta x}\Big(\widetilde{F}^+_{i-1/2}(t) - \widetilde{F}^-_{i+1/2}(t)\Big), \tag{3.2}$$

where the numerical fluxes are

$$\widetilde{F}^-_{i+1/2}(t) = F(U^-_{i+1/2}(t)) - F(U^+_i(t)) - I^-_{i+1/2}(t) + \widetilde{P}^-_{i+1/2}\Big(\widetilde{A}_{i+1/2}(U^+_{i+1/2}(t) - U^-_{i-1/2}(t)) - \widetilde{S}_{i+1/2}\Big) \tag{3.3}$$

and

$$\widetilde{F}^+_{i+1/2}(t) = F(U^+_{i+1/2}(t)) - F(U^-_{i+1}(t)) - I^+_{i+1/2}(t) - \widetilde{P}^+_{i+1/2}\Big(\widetilde{A}_{i+1/2}(U^+_{i+1/2}(t) - U^-_{i+1/2}(t)) - \widetilde{S}_{i+1/2}\Big). \tag{3.4}$$

Let us explain the notation used in the above expressions. First, define $U_i(t) = [h^t_i, q^t_i]^{\mathrm{T}}$ and $U^\pm_{i+1/2}(t) = [h^{\pm,t}_{i+1/2}, q^{\pm,t}_{i+1/2}]^{\mathrm{T}}$, so $W_i(t) = [U_i(t), H^t_i]^{\mathrm{T}}$ and $W^\pm_{i+1/2}(t) = [U^\pm_{i+1/2}(t), H^{\pm,t}_{i+1/2}]^{\mathrm{T}}$. Then $A_{i+1/2}$ and $\widetilde{P}^\pm_{i+1/2}$ are defined as in Section 2, using $U^+_{i+1/2}(t)$ and $U^-_{i+1/2}(t)$ instead of U^n_{i+1} and U^n_i, respectively. Besides, denote

$$\mathcal{R}^{\pm,t}_{i+1/2}(x) = \begin{bmatrix} r^{\pm,t}_{h,i+1/2}(x) \\ r^{\pm,t}_{q,i+1/2}(x) \\ r^{\pm,t}_{H,i+1/2}(x) \end{bmatrix}$$

and define $R^{\pm,t}_{i+1/2}(x) = [r^{\pm,t}_{h,i+1/2}(x), r^{\pm,t}_{q,i+1/2}(x)]^{\mathrm{T}}$. The approximations at the cell center x_i are then given by

$$U^+_i(t) = \lim_{x\to x_i^+} R^{t,-}_{i+1/2}(x), \quad U^-_{i+1}(t) = \lim_{x\to x_{i+1}^-} R^{t,+}_{i+1/2}(x).$$

The reconstructed numerical source term at the intercell is defined as

$$\widetilde{S}_{i+1/2} = \begin{bmatrix} 0 \\ \frac{g}{2}(h^{+,t}_{i+1/2} + h^{-,t}_{i+1/2})(H^{+,t}_{i+1/2} - H^{-,t}_{i+1/2}) \end{bmatrix},$$

while in the cells is approximated by

$$I^-_{i+1/2}(t) = \begin{bmatrix} 0 \\ \int_{x_i}^{x_{i+1/2}} gr^{-,t}_{h,i+1/2}(x)\frac{\mathrm{d}}{\mathrm{d}x} r^{-,t}_{H,i+1/2}(x)\,\mathrm{d}x \end{bmatrix} \tag{3.5}$$

and

$$I^+_{i+1/2}(t) = \begin{bmatrix} 0 \\ \int_{x_{i+1/2}}^{x_{i+1}} gr^{+,t}_{h,i+1/2}(x)\frac{\mathrm{d}}{\mathrm{d}x} r^{+,t}_{H,i+1/2}(x)\,\mathrm{d}x \end{bmatrix}. \tag{3.6}$$

In practice, the definition of the reconstruction operator provides a natural choice of the functions $\mathcal{R}^{\pm,t}_{i+1/2}$, as the usual procedure for defining a reconstruction operator is the following: given a sequence $\{W_i\}$ of values at the cells, first an approximating function is constructed at the subcell $[x_i, x_{i+1/2}]$, based on the values of W_i at a given stencil:

$$\mathcal{R}^-_{i+1/2}(x; W_{i-l}, \ldots, W_{i+r}),$$

for some natural numbers l, r. This function is calculated by means of interpolation or approximation procedures. Once $\mathcal{R}^-_{i+1/2}$ has been constructed, $W^-_{i+1/2}$ is calculated by taking the limit of $\mathcal{R}^-_{i+1/2}$ to the left of $x_{i+1/2}$. If the reconstruction operator is built following this procedure (as we will assume in the sequel), the natural choice of $\mathcal{R}^{-,t}_{i+1/2}$ would be

$$\mathcal{R}^{-,t}_{i+1/2}(x) = \mathcal{R}^-_{i+1/2}(x; W_{i-l}(t), \ldots, W_{i+r}(t)).$$

The operator $\mathcal{R}^{+,t}_{i+1/2}$ is constructed in an analogous way.

The order of the numerical scheme (3.1) is stated in the following result [8]:

Theorem 3.2. *Assume that $\mathcal{A}$ is of class $\mathcal{C}^2$ with bounded derivatives and $\mathcal{A}$ is also bounded. Suppose also that the p-order reconstruction operator is such that, given a sequence defined by*

$$W_i = \frac{1}{\Delta x}\int_{x_{i-1/2}}^{x_{i+1/2}} W(x)\,\mathrm{d}x$$

for some smooth function $W(x)$, we have that

$$\mathcal{R}^-_{i+1/2}(x; W_{i-l}, \ldots, W_{i+r}) = W(x) + \mathrm{O}(\Delta x^q), \quad x \in [x_i, x_{i+1/2}],$$
$$\frac{\mathrm{d}}{\mathrm{d}x}\mathcal{R}^-_{i+1/2}(x; W_{i-l}, \ldots, W_{i+r}) = W'(x) + \mathrm{O}(\Delta x^s), \quad x \in [x_i, x_{i+1/2}],$$

for some $q, s \geqslant 0$ (analogously for $\mathcal{R}^+_{i+1/2}$). Then (3.1) is an approximation of order at least $\gamma = \min(p, q+1, s+1)$ to the system (2.2) in the following sense:

$$\begin{aligned}
&\mathcal{A}^+_{i-1/2}(W^+_{i-1/2}(t) - W^-_{i-1/2}(t)) + \mathcal{A}^-_{i+1/2}(W^+_{i+1/2}(t) - W^-_{i+1/2}(t)) + \int_{x_{i-1/2}}^{x_i} \mathcal{A}(\mathcal{R}^{+,t}_{i-1/2}(x))\frac{\mathrm{d}}{\mathrm{d}x}\mathcal{R}^{+,t}_{i-1/2}(x)\,\mathrm{d}x \\
&\quad + \int_{x_i}^{x_{i+1/2}} \mathcal{A}(\mathcal{R}^{-,t}_{i+1/2}(x))\frac{\mathrm{d}}{\mathrm{d}x}\mathcal{R}^{-,t}_{i+1/2}(x)\,\mathrm{d}x \\
&\quad = \int_{x_{i-1/2}}^{x_{i+1/2}} \mathcal{A}(W(x,t))W_x(x,t)\,\mathrm{d}x + \mathrm{O}(\Delta x^\gamma),
\end{aligned}$$

for every smooth enough solution $W(x,t)$, being $W^{\pm}_{i+1/2}(t)$ the associated reconstructions and $\mathcal{R}^{\pm,t}_{i+1/2}(x)$ the approximation functions corresponding to the sequence of cell averages

$$W_i(t) = \frac{1}{\Delta x}\int_{x_{i-1/2}}^{x_{i+1/2}} W(x,t)\,\mathrm{d}x.$$

Remark 3.3. In practice we will usually have $q \leqslant p$ and $s = q - 1$. For example, if WENO reconstructions [19,23] with stencils of n points are considered then $p = 2n - 1$, $q = n$ and $s = n - 1$, so the order of the scheme is $\gamma = n$. This loss of accuracy is caused by the integral terms appearing in (3.1), as they involve reconstructed values on the whole cell I_i and not only at the intercells. If ENO reconstructions [18] with stencils of n points are used, we have $p = q = n$ and $r = n - 1$, so $\gamma = n$. In this case there is no order reduction.

In [8] it is also proved that, under the hypotheses of Theorem 3.2, the scheme (3.1) is exactly well-balanced for still water solutions and well-balanced with order γ for general stationary solutions.

Finally, in order to have a fully discretized scheme, an adequate high order scheme has to be applied to (3.1) for time-stepping. In practice, we will consider the TVD Runge–Kutta schemes proposed in [15,31].

4. The MRoe scheme for shallow water equations

Recently, in [9] a new technique for dealing with the appearance of wet/dry areas when solving the shallow water system (2.1) has been developed. This technique consists in replacing, at the intercells where a wet/dry transition is detected, the approximate linear Riemann problem by a nonlinear one, that is exactly solved. In these Riemann problems, one of the initial states corresponds to vacuum (vacuum Riemann problems have also been used in [25] in the context of gas dynamics). The construction of the *modified Roe scheme* (MRoe in the sequel) is summarized in this section.

We consider the form (2.8) of the Roe scheme, as it is more convenient in this context than the general form (2.6). From time t^n, the MRoe scheme advances in time using (2.8) with the following modification of the numerical fluxes:

- If there is no wet/dry transition at the intercell $x_{i+1/2}$, the fluxes are still given by (2.9).
- If a wet/dry transition is detected at $x_{i+1/2}$, the fluxes are defined as

$$F^-_{i+1/2} = F(U^-_{i+1/2}), \quad F^+_{i+1/2} = F(U^+_{i+1/2}),$$

where $U^-_{i+1/2}$ and $U^+_{i+1/2}$ are the limits to the left and to the right of $x_{i+1/2}$ of the solution of an appropriate nonlinear Riemann problem.

Assume that a wet/dry transition has been detected at $x_{i+1/2}$ at time t^n. Without loss of generality, let us suppose that the cell I_i is wet and I_{i+1} is dry, i.e., $h^n_i > 0$ and $h^n_{i+1} = 0$ (the description of the solutions in the opposite case are similar). For the sake of simplicity, we also assume that $x_{i+1/2} = 0$ and $t^n = 0$. The left state W^n_i is denoted by $W_{\mathrm{L}} = [h_{\mathrm{L}}, q_{\mathrm{L}}, H_{\mathrm{L}}]^{\mathrm{T}}$, while the right state W^n_{i+1} has the form $W_{\mathrm{R}} = [0, 0, H_{\mathrm{R}}]^{\mathrm{T}}$. We also define $u_{\mathrm{L}} = q_{\mathrm{L}}/h_{\mathrm{L}}$ and $c_{\mathrm{L}} = \sqrt{g h_{\mathrm{L}}}$. Finally, let W^- and W^+ denote the left and right limits at $x = 0$ of the solution of the nonlinear Riemann problem to be solved associated to the interface.

We summarize now the possible values of $W^{\pm}$, depending on the relation between H_{L} and H_{R}. The details can be found in [9].

- Case 1: $H_{\mathrm{L}} = H_{\mathrm{R}}$ (flat bottom). As the bottom is constant in this case, the equations (2.1) form a system of conservation laws in the variables $U = [h, q]^{\mathrm{T}}$, so the usual Riemann problem is considered:

$$\begin{cases} U_t + F(U)_x = 0, \\ U(x,0) = \begin{cases} U_{\mathrm{L}} & \text{if } x < 0, \\ U_{\mathrm{R}} & \text{if } x > 0. \end{cases} \end{cases} \tag{4.1}$$

The solution of this problem is continuous (see, e.g. [33]) and its value at $x = 0$ is given by

$$U^{\pm} = \begin{bmatrix} h_0 \\ q_0 \end{bmatrix} = \begin{cases} [0,0]^{\mathrm{T}} & \text{if } u_{\mathrm{L}} \leqslant -2c_{\mathrm{L}}, \\ \left[\frac{(u_{\mathrm{L}}+2c_{\mathrm{L}})^2}{9g}, \frac{(u_{\mathrm{L}}+2c_{\mathrm{L}})^3}{27g}\right]^{\mathrm{T}} & \text{if } -2c_{\mathrm{L}} \leqslant u_{\mathrm{L}} \leqslant c_{\mathrm{L}}, \\ U_{\mathrm{L}} & \text{if } u_{\mathrm{L}} \geqslant c_{\mathrm{L}}. \end{cases} \tag{4.2}$$

The states $W^- = [U^-, H_{\mathrm{L}}]^{\mathrm{T}}$ and $W^+ = [U^+, H_{\mathrm{R}}]^{\mathrm{T}}$ are then considered.

- Case 2: $H_{\mathrm{L}} < H_{\mathrm{R}}$ (decreasing bottom). The following nonlinear Riemann problem is considered at the interface:

$$\begin{cases} W_t + \mathcal{A}(W)W_x = 0, \\ W(x,0) = \begin{cases} W_{\mathrm{L}} & \text{if } x < 0, \\ W_{\mathrm{R}} & \text{if } x > 0. \end{cases} \end{cases} \tag{4.3}$$

The simple waves corresponding to this nonconservative system are:

– rarefaction waves connecting states with the same value of H, which are identical to the usual rarefaction waves of the conservative problem;
– shocks linking states with the same value of H and satisfying the usual Rankine–Hugoniot conditions;
– stationary contact discontinuities joining two states that belong to the same curve of the family (2.3).

For $t > 0$ and $x < 0$, the solution obtained in Case 1 is still valid here. Thus, we have a rarefaction wave connecting W_{L} with the state $W_0 = [h_0, q_0, H_{\mathrm{L}}]^{\mathrm{T}}$, where h_0 and q_0 are given by (4.2). Next, W_0 is connected with a new state $W_1 = [h_1, q_1, H_{\mathrm{R}}]^{\mathrm{T}}$ through a stationary contact discontinuity. Finally, W_1 is linked to W_{R} using another rarefaction wave.

The limits of the solution of the nonlinear Riemann problem at $x = 0$ are given by

$$W^- = \begin{bmatrix} h_0 \\ q_0 \\ H_{\mathrm{L}} \end{bmatrix}, \quad W^+ = W_1 = \begin{bmatrix} h_1 \\ q_1 \\ H_{\mathrm{R}} \end{bmatrix}. \tag{4.4}$$

There are three cases to consider:

- If $u_{\mathrm{L}} \leqslant c_{\mathrm{L}}$ then $h_1 = 0$ and $q_1 = 0$.
- If $-2c_{\mathrm{L}} \leqslant u_{\mathrm{L}} \leqslant c_{\mathrm{L}}$ then h_1 is the largest root of the polynomial

$$P_0(h) = h^3 + \left(H_{\mathrm{L}} - H_{\mathrm{R}} - \frac{q_0^2}{2gh_0^2} - h_0\right)h^2 + \frac{q_0^2}{2g}$$

and $q_1 = q_0$.
- If $u_{\mathrm{L}} \geqslant c_{\mathrm{L}}$ then h_1 is the smallest positive root of the polynomial

$$P_{\mathrm{L}}(h) = h^3 + \left(H_{\mathrm{L}} - H_{\mathrm{R}} - \frac{q_{\mathrm{L}}^2}{2gh_{\mathrm{L}}^2} - h_{\mathrm{L}}\right)h^2 + \frac{q_{\mathrm{L}}^2}{2g} \tag{4.5}$$

and $q_1 = q_{\mathrm{L}}$.

Remark 4.1. In the case $-2c_{\mathrm{L}} \leqslant u_{\mathrm{L}} \leqslant c_{\mathrm{L}}$ the state W^- is critical and it can be linked to two different states through a contact discontinuity, one of them subcritical and the other one supercritical. Therefore the solution of the Riemann problem is not unique. We choose the subcritical one in order to avoid a transition (the states at $x < 0$ are subcritical). That is the reason why we choose the largest positive root of $P_0(h)$.

- Case 3: $H_L > H_R$ (emerging bottom). As it was noticed in [9], in this case the Riemann problem (4.3) may have no solution. Some different cases must be distinguished:

  Case 3.1: The step acts as an obstacle for the fluid. This happens if

- $u_L \leqslant 0$ and $H_R \leqslant H_L - h_L$; or
- $u_L \geqslant 0$ and

$$H_L - H_R > h_L + \frac{q_L^2}{2gh_L^2} - \frac{3q_L^{2/3}}{2g^{1/3}}.$$

The above condition means that the mechanical energy at the wet cell is not enough to make the fluid go up the step.

In this case, the following partial Riemann problem is considered:

$$\begin{cases} U_t + F(U)_x = 0, \\ U(x,0) = U_L & \text{if } x < 0, \\ U(x,0) \in \mathcal{V}_R & \text{if } x > 0, \end{cases} \tag{4.6}$$

where $\mathcal{V}_R = \{[h,0]^T : h \geqslant 0\}$. Its solution can be calculated using the theory developed in [12]. The limits of the solution at $x = 0$ are given by

$$W^- = \begin{bmatrix} \tilde{h} \\ 0 \\ H_L \end{bmatrix}, \quad W^+ = \begin{bmatrix} 0 \\ 0 \\ H_R \end{bmatrix}, \tag{4.7}$$

where the value $\tilde{h}$ is defined as follows:

- If $u_L \leqslant -2c_L$ then $\tilde{h} = 0$. In this case, the solution of (4.6) consists of a rarefaction wave connecting U_L to the vacuum state.
- If $-2c_L < u_L \leqslant 0$ then

$$\tilde{h} = \frac{1}{g}\left(\frac{u_L}{2} + c_L\right)^2.$$

Here, the solution of (4.6) is a rarefaction wave linking U_L with a constant state region where the flow is at rest and $h = \tilde{h}$.

- If $u_L > 0$ then $\tilde{h}$ is the largest root of the polynomial

$$P(h) = h^3 - h_L h^2 - h_L^2 h + h_L^3 - \frac{2h}{gh_L} q_L^2.$$

In this case the solution of (4.6) is an entropic shock linking U_L with $[\tilde{h}, 0]^T$.

Case 3.2: The flow at the wet cell is supercritical, it advances towards the step and it has mechanical energy enough to go up the step, i.e., $u_L > 0$ and

$$H_L - H_R < h_L + \frac{q_L^2}{2gh_L^2} - \frac{3q_L^{2/3}}{2g^{1/3}}.$$

In this case the solution of the nonlinear Riemann problem (4.3) can be easily calculated. Its structure is the following: first a contact discontinuity is considered which connects W_L with the state $[h_1, q_L, H_R]^T$, where h_1 is the smallest positive root of the polynomial $P_L(h)$ given by (4.5); then, this state is linked to $[0, 0, H_R]^T$ through another rarefaction wave. Thus we obtain:

$$W^- = W_{\mathrm{L}}, \quad W^+ = \begin{bmatrix} h_1 \\ q_{\mathrm{L}} \\ H_{\mathrm{R}} \end{bmatrix}. \tag{4.8}$$

Case 3.3: In the remaining cases the flow has energy enough to go up the step, but the problem (4.3) cannot be solved as easily as in the previous cases. In such situations, the scheme (2.8) is applied without modifications.

We finish this section remarking two important properties of the MRoe scheme (their proofs can be found in [9]):

Proposition 4.2. *The MRoe scheme is well-balanced in the sense that it exactly solves the steady state solutions corresponding to water at rest, including or not wet/dry situations.*

Proposition 4.3. *The positivity of the value of h produced at the cells where a wet/dry front has been detected is assured except in case* 3.3, *where the scheme (2.8) is applied with no further modifications. In this latter case, a restriction on the CFL condition can be considered in order to warrant the positivity of h.*

5. High-order extension of the MRoe scheme

We develop in this section a well-balanced finite volume scheme for solving (2.1) that is capable of handling wet/dry situations, being at the same time high-order accurate in smooth wet areas. As it was commented in Section 1, the construction of such scheme is the main result of this article.

The ingredients to construct the scheme have been developed in Sections 3 and 4. The idea is to combine the high order scheme (3.2) with the MRoe technique for treating wet/dry situations. The resulting scheme will be called the *High-order MRoe* (HMRoe in the sequel) scheme.

The first step is to select adequate variables to be reconstructed. As it was done in [8], in order to have an exactly well-balanced scheme for water at rest solutions, the surface elevation $\eta = h - H$ has to be reconstructed. On the other hand, it is also important to choose a reconstruction of the water height h that preserves positivity. Thus, the variables considered are (h, q, η); if $(\tilde{h}, \tilde{q}, \tilde{\eta})$ represent the reconstructed values, the reconstructed depth is then defined as $\tilde{H} = \tilde{h} - \tilde{\eta}$.

We give now a complete description of the semidiscrete HMRoe scheme. First of all, a tolerance h_ε must be fixed in order to distinguish between wet and dry cells. Assume that the cell averages $W_i = [h_i, q_i, H_i]^{\mathrm{T}}$ at a given time t are known (for the sake of clarity, dependence on time is dropped). Then:

Reconstruction step

- Define the cell averages $\eta_i = h_i - H_i$.
- Use the cell averages on an adequate stencil to build reconstructing functions for each variable $\alpha \in \{h, q, \eta\}$:

  $$r^-_{\alpha,i+1/2}(x),\ x \in [x_i, x_{i+1/2}]; \quad r^+_{\alpha,i+1/2}(x),\ x \in [x_{i+1/2}, x_{i+1}],$$

  and compute the reconstructed values at the intercell:

  $$\alpha^\pm_{i+1/2} = r^\pm_{\alpha,i+1/2}(x_{i+1/2}),\ \alpha \in \{h, q, \eta\}.$$

  Define also

  $$r^\pm_{H,i+1/2}(x) := r^\pm_{h,i+1/2} - r^\pm_{\eta,i+1/2}(x),$$

  and consider the reconstruction operators

  $$R^\pm_{i+1/2}(x) = [r^\pm_{h,i+1/2}(x), r^\pm_{q,i+1/2}(x)]^{\mathrm{T}}.$$

The reconstructed states at the intercell are $U^\pm_{i+1/2} = [h^\pm_{i+1/2}, q^\pm_{i+1/2}]^{\mathrm{T}}$; also, define $W^\pm_{i+1/2} = [U^\pm_{i+1/2}, H^\pm_{i+1/2}]^{\mathrm{T}}$, where $H^\pm_{i+1/2} := h^\pm_{i+1/2} - \eta^\pm_{i+1/2}$.

- If a stencil contains a dry cell, simply take $W^-_{i+1/2} = W^n_i$ or $W^+_{i+1/2} = W^n_{i+1}$, depending on the case. Notice that this causes a loss of accuracy near a wet/dry front.
- The reconstructed velocity is defined as $u^\pm_{i+1/2} = q^\pm_{i+1/2}/h^\pm_{i+1/2}$; however, in order to avoid cancellation problems near a wet/dry front, we set $u^\pm_{i+1/2} = 0$ if $h^\pm_{i+1/2} < h_\varepsilon$.

Numerical fluxes

- In the wet-bed case, the numerical fluxes $\widetilde{F}^\pm_{i+1/2}$ are defined by (3.3) and (3.4).
- If a wet/dry transition is detected, apply the technique introduced in Section 4 with the states $W_L = W^-_{i+1/2}$ and $W_R = W^+_{i+1/2}$. Denote by $\widetilde{W}^+_{i+1/2}$ and $\widetilde{W}^-_{i+1/2}$ the states given by (4.2), (4.4), (4.7), or (4.8), depending on the case (in Case 3.3, we simply take $\widetilde{W}^\pm_{i+1/2}$ as $W^\pm_{i+1/2}$). Then the numerical fluxes $\widetilde{F}^\pm_{i+1/2}$ are defined again by (3.3) and (3.4) using $\widetilde{W}^\pm_{i+1/2}$, except in Case 3.1 where we take

$$\widetilde{F}^-_{i+1/2}(t) = F(U^-_{i+1/2}(t)) - F(U^+_i(t)),$$
$$\widetilde{F}^+_{i+1/2}(t) = F(U^+_{i+1/2}(t)) - F(U^-_{i+1}(t)),$$

due to the fact that the Riemann problem (4.6) does not involve the effects of the source term directly in the equation.

Once the semidiscrete scheme has been defined, the system (3.2) is discretized in time by using a standard solver.

Following the results in [8,9], the HMRoe scheme is exactly well-balanced for water at rest solutions (including or not dry areas), and well-balanced with the same accuracy of the reconstruction operator for general stationary solutions.

On the other hand, notice that the positivity of the reconstruction of h is not sufficient to guarantee the positivity of the scheme. However, from Proposition 4.3 we can deduce that the HMRoe scheme preserves the positivity of h, although in same cases a restriction on the CFL condition may be needed.

6. Choice of the reconstruction operator: the hyperbolic HMRoe scheme

In [8] parabolic WENO reconstruction operators [19] were considered for the implementation of the high-order scheme (3.1) in wet domains, providing very good results. However, when dry or almost dry areas are present, the non-monotone character of parabolas may lead to negative (non-physical) values of the water height h (even though the WENO technique provides a way for damping oscillations, this is not sufficient in general for avoiding the appearance of negative values of h). Although in the experiments performed the negative values of h are relatively small, they may lead the computer program to crash.

Instead of reconstructions of parabolic type, we will focus here on third-order *hyperbolic* reconstructions. Specifically, Marquina's local hyperbolic harmonic method (LHHR) introduced in [24] will be applied. This method prescribes at each cell I_i a hyperbola that preserves the cell-average, interpolates the lateral derivative of the solution with smaller absolute value, and assigns as the central derivative the harmonic mean of the lateral derivatives. This method is LTVB (local total variation bounded), that is, the total variation of each hyperbola is bounded by $M\Delta x$, for some constant M. Details on the method can be found in [24].

Remark 6.1. The main drawback of the LHHR method is the loss of total variation at local extrema, produced by a loss of accuracy at those points. Indeed, when the harmonic limiter is used the reconstruction may degenerate to second-order near extrema. Some improvements on this point can be achieved by choosing different kinds of limiters: see [30]. However, in our numerical experiments the best results have been obtained when the harmonic limiter is used, specially near wet/dry fronts.

Remark 6.2. There is also relevant recent work on extensions of hyperbolic reconstructions in [1]. Applications of this new kind of reconstructions within the HMRoe framework are currently under investigation.

The main reasons for choosing hyperbolic reconstructions are listed below:

- Positivity: if the values of the cell averages of h are non-negative at each cell of the stencil, the reconstructed value is also non-negative (for the sake of clarity in the presentation, the proof of this fact has been included in the Appendix).
- The reconstructions are third-order accurate on the whole cell I_i (except at local extrema, where the accuracy may degenerate to second-order; see Remark 6.1). Thus, from the results of Section 3 (we would have $p = q = 3$ and $r = 2$, so $\gamma = 3$ in Theorem 3.2) the scheme will be also third-order accurate on smooth wet areas and well-balanced with order three for general stationary solutions.
- Compactness of the stencil. Each hyperbola is constructed using only three cell-values (while, for example, a parabolic WENO method needs five cell-values for each lateral reconstruction). This makes the method to work robustly when used with shock-capturing schemes, and allows an easier analysis of wet/dry situations.
- The total variation of hyperbolas are much smaller then those of parabolas, thus reducing the oscillating behaviour near shocks.

Finally, for time discretization a third-order TVD Runge–Kutta method [31,15] has been considered.

7. A two-dimensional extension of the HMRoe scheme in quadrilateral meshes

A natural extension of Marquina's hyperbolic reconstruction method to non-uniform meshes in two space dimensions has been recently introduced in [29]. This extension, known as the *bi-hyperbolic* method, considers at each computational cell a combination of two hyperbolas obtained using the LHHR algorithm in both spatial directions. When quadrilateral (not necessarily uniform) meshes are used, the bi-hyperbolic method provides a third-order reconstruction on the whole cell.

The bi-hyperbolic method allows to extend the HMRoe scheme to a two-dimensional setting on quadrilateral meshes, as the technique introduced in Section 4 can be applied componentwise with no further modifications. As stated in [29], third-order of accuracy is reached on smooth wet regions; however, only first-order of accuracy can be expected near shocks and wet/dry transitions. Positivity of the water height is also preserved, under an appropriate CFL restriction.

8. Numerical experiments

In this section we test the performance of the hyperbolic HMRoe scheme defined in Section 6. The integral terms (3.5) and (3.6) are approximated by means of a Gaussian quadrature with three points. The CFL number is set to 0.9 unless otherwise stated. The wet/dry tolerance h_ε has been taken as 10^{-6} and the gravity constant is $g = 9.81$.

8.1. Exact well-balance property for still water solutions

We consider a simple test to verify that solutions corresponding to water at rest including a wet/dry transition are exactly computed with the HMRoe scheme.

The bottom consists of an obstacle defined by the depth function [36]

$$H(x) = 10 - 5\mathrm{e}^{-0.4(x-5)^2}, \quad 0 \leqslant x \leqslant 10,$$

and the initial water height has been taken as 2.5 on both sides of the obstacle (see Fig. 1). The HMRoe scheme has been run until time $t = 0.5$ using a mesh with 200 nodes.

As expected, the scheme preserves the stationary solution up to round-off error. Indeed, the L^1 errors obtained for h and q using double precision are, respectively, 4.08E−14 and 5.75E−14.

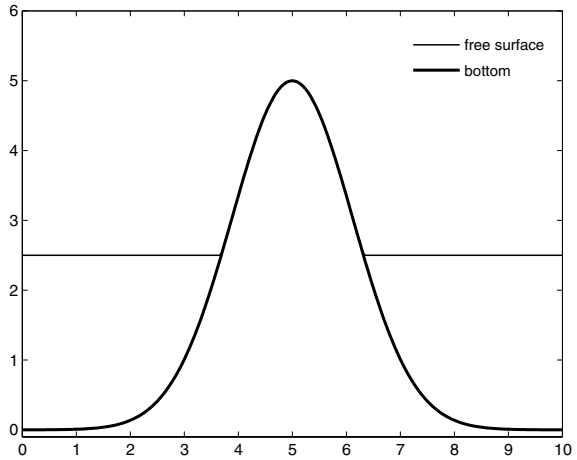

Fig. 1. Flow at rest. Bottom topography and free surface elevation computed with the HMRoe scheme at time $t = 0.5$.

8.2. One-dimensional accuracy test

A test proposed in [36] is considered here to measure the accuracy of the HMRoe scheme. The problem is defined by the bottom function

$$H(x) = 2 - \sin^2(\pi x), \quad x \in [0, 1],$$

and the initial conditions

$$h(x, 0) = 5 + e^{\cos(2\pi x)}, \quad q(x, 0) = \sin(\cos(2\pi x)),$$

imposing periodic boundary conditions. As the exact solution for this test is not known, in order to compute the numerical errors we have considered a reference solution calculated using the HMRoe scheme with 6400 nodes.

The solutions have been computed up to time $t = 0.1$, when the solution still remains smooth. Table 1 shows the L^1 errors and numerical orders of accuracy obtained with CFL number 0.8. As expected, we do not get full third-order of accuracy for this test. The reason is that monotone reconstructions as LHHR suffer from clipping of extrema leading to a loss of global accuracy. For comparison, we have also included the results obtained with the first order MRoe scheme in Table 2.

8.3. Dambreak over a plane

The ability of the HMRoe scheme for computing the advance of wet/dry fronts is tested in the experiments considered in this section, that were previously analyzed in [9]. The computational domain considered is the interval [−15,15] and the bottom is given by the depth function

$$H(x) = 1 - x\tan(\alpha),$$

Table 1
HMRoe scheme

Number of cells	L^1 error h	L^1 order h	L^1 error q	L^1 order q
100	1.7E−03	–	1.4E−02	–
200	2.7E−04	2.65	2.4E−03	2.62
400	4.8E−05	2.50	4.4E−04	2.44
800	8.3E−06	2.55	7.3E−05	2.57
1600	1.4E−06	2.61	1.2E−05	2.60

One-dimensional accuracy test. L^1 numerical errors and orders.

Table 2
MRoe scheme

Number of cells	L^1 error h	L^1 order h	L^1 error q	L^1 order q
100	2.7E−02	–	1.6E−01	–
200	1.5E−02	0.89	8.9E−02	0.89
400	7.7E−03	0.94	4.7E−02	0.93
800	4.0E−03	0.96	2.4E−02	0.95
1600	2.0E−03	0.98	1.2E−02	0.97

One-dimensional accuracy test. L^1 numerical errors and orders.

for some angle α. The initial conditions considered are

$$q(x,0)=0, \quad h(x,0)=\begin{cases} H(x) & \text{if } x<0, \\ 0 & \text{otherwise.} \end{cases}$$

With regard to the boundary conditions, the discharge $q(0, t) = 0$ is imposed at $x = -15$ while a free boundary condition is considered at $x = 15$. The space step has been taken as $\Delta x = 0.05$.

For this problem, the exact position and velocity of the advancing wet/dry front can be exactly computed (see [9]):

$$x_f(t) = 2t\sqrt{gh_0\cos(\alpha)} - \frac{1}{2}gt^2\tan(\alpha),$$
$$u_f(t) = 2\sqrt{gh_0\cos(\alpha)} - gt\tan(\alpha),$$

where $h_0 = 1$ in this case.

Depending on the sign of $\tan(\alpha)$, three different kinds of wet/dry fronts may appear. As in [9], we consider the values $\alpha = 0$ (flat bottom), $\alpha = \pi/60$ (emerging topography) and $\alpha = -\pi/60$ (bottom with increasing depth). The topography and free surface of the fluid at time $t = 0$ in the case $\alpha = \pi/60$ are represented in Fig. 2.

The time evolution until $t = 2$ of the positions of the wet/dry fronts for each experiment are shown in Figs. 3a, c and e; the corresponding velocities are depicted in Figs. 3b, d and f. As it can be seen, the HMRoe scheme produces more accurate results than the MRoe scheme. Also, in Fig. 4, a comparison with the analytical solution near the wet/dry front in the case $\alpha = 0$ is also shown.

The analysis of CPU times shows that, in the three cases considered, the MRoe scheme is about four times faster than the HMRoe scheme.

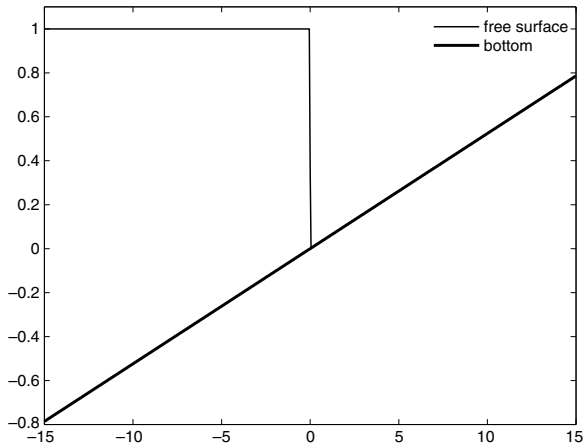

Fig. 2. Dambreak problem over a non-flat bottom (case $\alpha = \pi/60$). Initial condition.

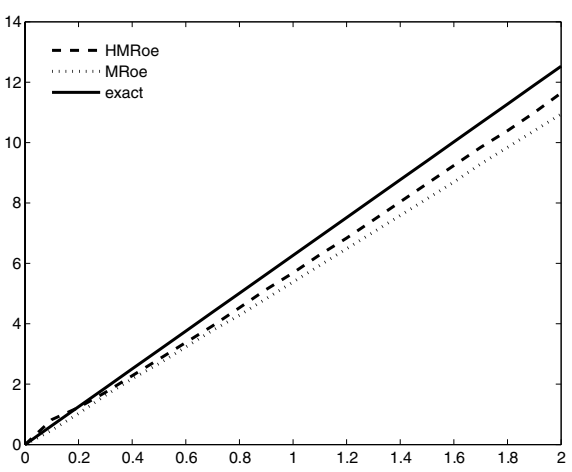

(a) $\alpha = 0$ (position).

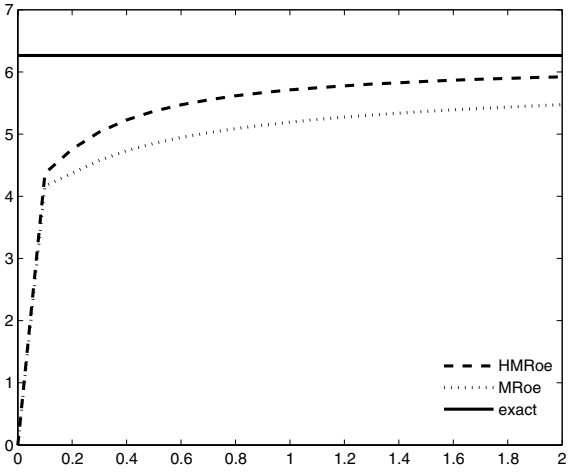

(b) $\alpha = 0$ (velocity).

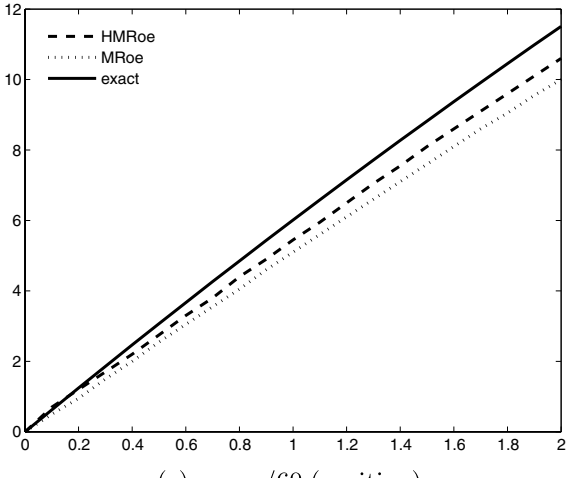

(c) $\alpha = \pi/60$ (position).

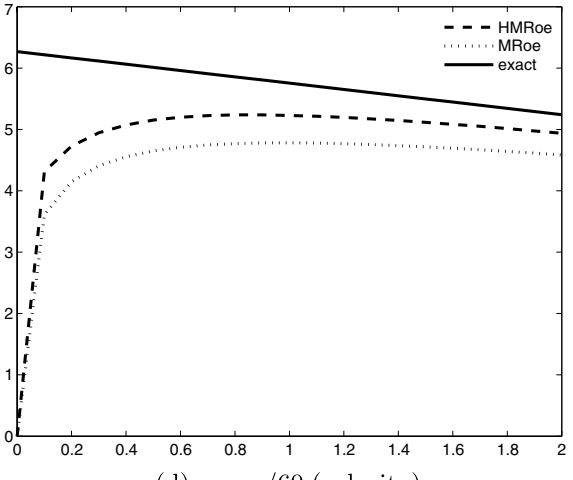

(d) $\alpha = \pi/60$ (velocity).

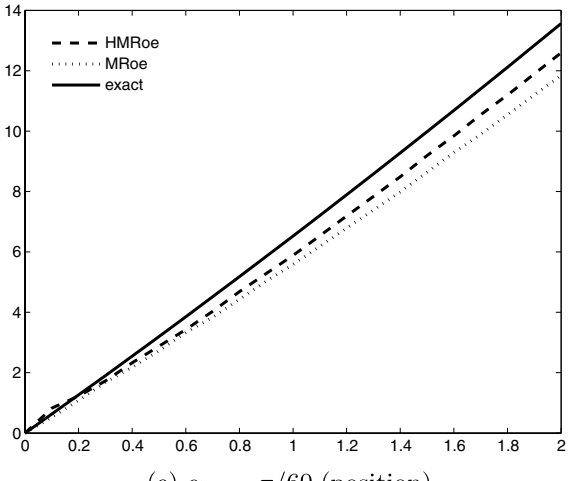

(e) $\alpha = -\pi/60$ (position).

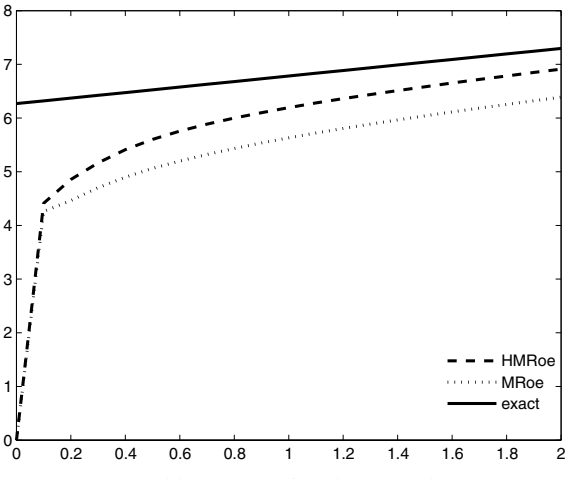

(f) $\alpha = -\pi/60$ (velocity).

Fig. 3. Dambreak over a plane. Left: front position vs. time. Right: front velocity vs. time.

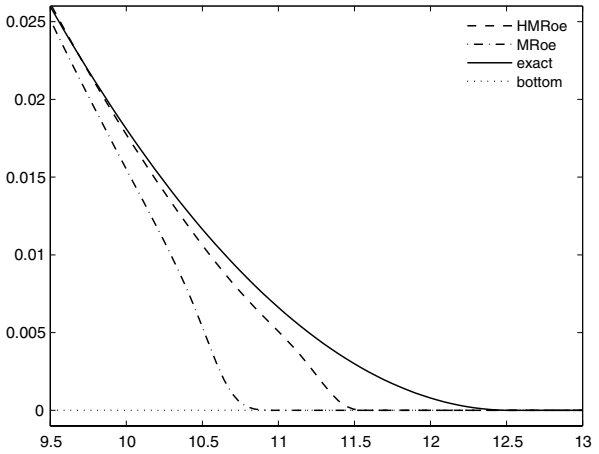

Fig. 4. Dambreak over a flat plane. Zoom of the wet/dry front.

8.4. Dry bed generation

We first consider an experiment over flat bottom proposed by Toro in [33]. The initial conditions are

$$h(x,0) = 0.1, \quad q(x,0) = \begin{cases} -0.3 & \text{if } x < 5, \\ 0.3 & \text{if } x > 5. \end{cases}$$

In this case, a dry bed is formed in the middle of two rarefactions waves travelling in opposite directions. The generation of the dry bed makes this problem numerically difficult.

The results obtained at time $t = 1$ with both the HMRoe and the MRoe schemes are compared with the exact solution in Figs. 5 and 6. The computational domain is the interval $[0, 10]$ and the space step is $\Delta x = 0.05$. In this case, the CFL number has been reduced to 0.8 in order to avoid the appearance of negative values of the water height (see Proposition 4.3). A zoom of the dry zone is shown in Fig. 7; as it can be observed, the MRoe scheme leaves a small wet zone between the two rarefaction waves. For this test, the HMRoe scheme consumes about three times the CPU time needed by the MRoe scheme.

Let us consider now a modification of the previous test by including a non-trivial topography. Specifically, we consider the test proposed in [13], where the depth function is given by

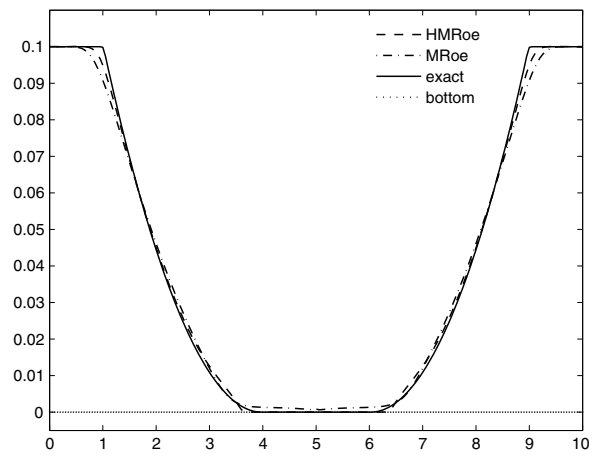

Fig. 5. Dry bed generation on a flat bottom. Free surface elevation at time $t = 1$.

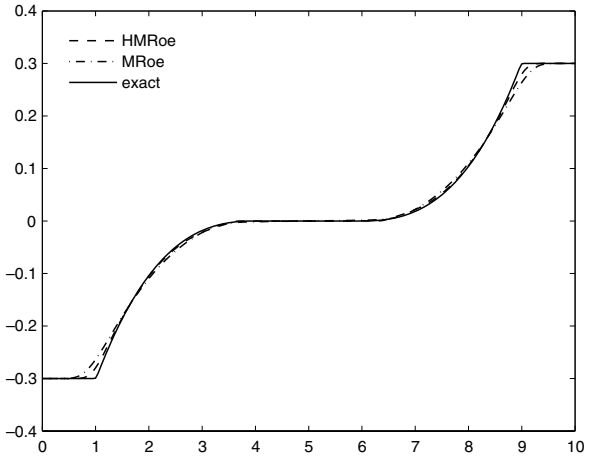

Fig. 6. Dry bed generation on a flat bottom. Discharge at time $t = 1$.

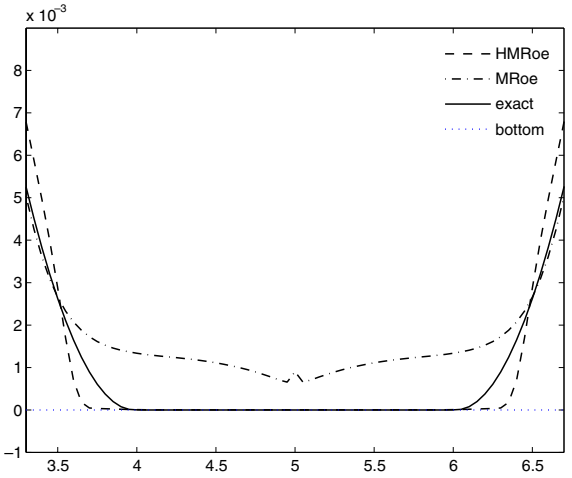

Fig. 7. Dry bed generation on a flat bottom. Zoom of the dry zone.

$$H(x) = \begin{cases} 13 & \text{if } 25/3 < x < 25/2, \\ 14 & \text{otherwise,} \end{cases}$$

in the domain $[0, 25]$. The initial water height is 10 and the initial discharge is

$$q(x,0) = \begin{cases} -350 & \text{if } x < 50/3, \\ 350 & \text{otherwise.} \end{cases}$$

The results obtained at times 0, 0.05, 0.25, 0.45 and 0.65, using 300 nodes and CFL number 0.8, are shown in Figs. 8 and 9. These results are in good agreement with those obtained in [13]. Regarding the CPU time, in this test the MRoe scheme is about four times faster.

8.5. Drain on a non-flat bottom

We consider the bottom topography defined by

$$H(x) = \begin{cases} 0.05(x-10)^2 & \text{if } 8 \leqslant x \leqslant 12, \\ 0.2 & \text{otherwise,} \end{cases}$$

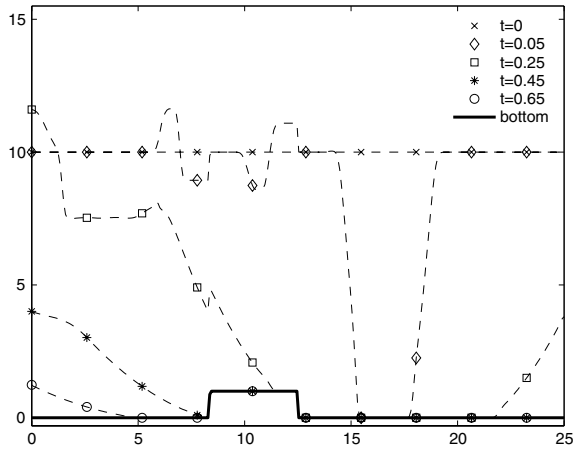

Fig. 8. Dry bed generation on a non-flat bottom. Free surface elevation obtained with the HMRoe scheme at different times.

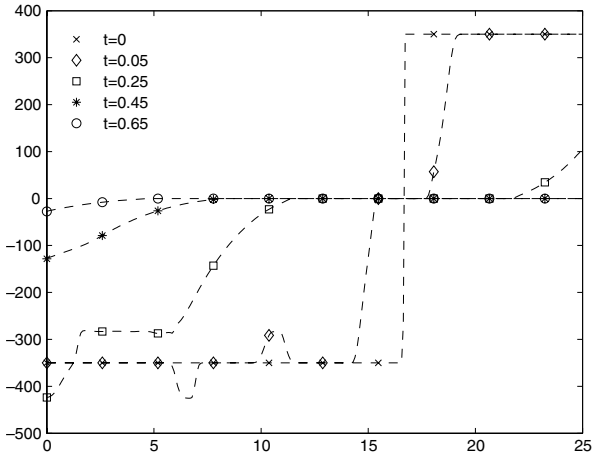

Fig. 9. Dry bed generation on a non-flat bottom. Discharge obtained with the HMRoe scheme at different times.

in the domain [0, 25], and initial conditions $h(x, 0) = H(x) + 0.3$ and $q(x, 0) = 0$. A free boundary condition is imposed on the left and an outlet condition on a dry bed (see [7]) on the right. The flow reaches a stationary state with $h = 0.2$ to the left of the bump and $h = 0$ to its right. This experiment was proposed in [13].

The HMRoe scheme has been applied with 300 nodes and CFL number 0.8, at times $t = 0$, 10, 20, 100 and 1000. The results obtained are shown in Figs. 10 and 11, and can be directly compared with those presented in [13].

8.6. Oscillating lake

The following experiment was proposed in [2]. The bottom topography given by

$$H(x) = 0.5^2(\cos(\pi(x - 0.5)/0.5) + 1), \quad x \in [0, 1],$$

simulates a lake bed with non-flat bottom and non-vertical shores. Initially, the water surface at rest is perturbed with a small sinusoidal wave:

$$h(x, 0) = \max\left[0, H(x) - 0.1 + 0.04\left(\sin\left(\frac{x - 0.5}{0.25}\right) + 0.04\max(0, 0.1 - H(x))\right)\right].$$

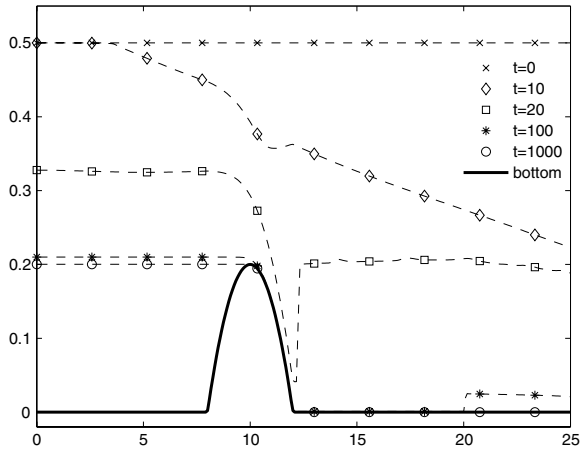

Fig. 10. Drain on a non-flat bottom. Free surface elevation computed using the HMRoe scheme at different times.

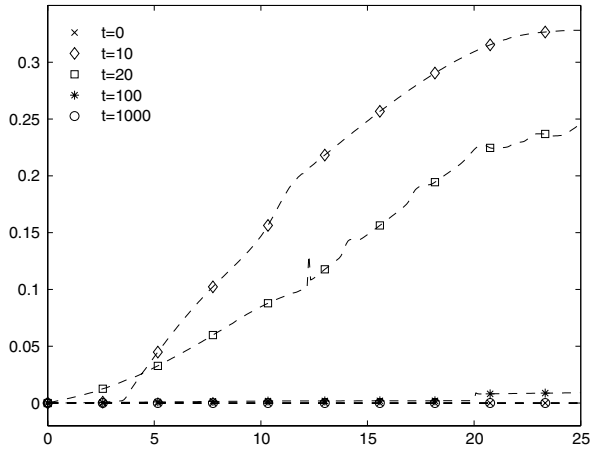

Fig. 11. Drain on a non-flat bottom. Discharge computed using the HMRoe scheme at different times.

Then the flow oscillates and, at each time step, an interface between wet and dry cells has to be computed at each shore. The results obtained with the HMRoe scheme at time $t = 19.87$, when the water reaches its higher level on the left shore, is shown in Fig. 12. We also observe that the scheme maintains the periodic regime for all time. The computations have been performed with 200 nodes and CFL number equal to 0.8.

8.7. Two-dimensional accuracy test

As it was done in the one-dimensional case, we consider a test proposed in [36] in order to measure the accuracy of the bi-hyperbolic HMRoe scheme. Specifically, the bottom topography is defined as

$$H(x,y) = 2 - \sin(2\pi x) - \cos(2\pi y),$$

the initial water height is

$$h(x,y,0) = 10 + e^{\sin(2\pi x)}\cos(2\pi y),$$

while the initial discharges are given by

$$q_1(x,y,0) = \sin(\cos(2\pi x))\sin(2\pi y), \quad q_2(x,y,0) = \cos(2\pi x)\cos(\sin(2\pi y)).$$

The computational domain is the unit square and periodic boundary conditions have been imposed.

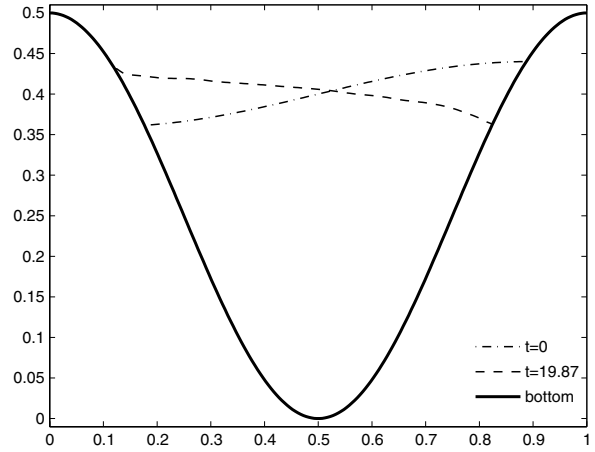

Fig. 12. Oscillating lake. Free surface elevation: initial condition and solution calculated with the HMRoe scheme at time $t = 19.87$.

Table 3 shows the results obtained at time $t = 0.05$, as shocks developed later for this problem. The solution computed with the bi-hyperbolic HMRoe scheme on a mesh with 800×800 grid points has been taken as reference solution. The CFL number has been taken as 0.5. As it can be seen, third-order of accuracy is achieved. Unlike the one-dimensional case, there is no order reduction due to local extrema, mainly due to the more suitable form of the bi-hyperbolic reconstructing functions.

8.8. Flooding on an open channel

We consider a topography based on [20], which represents a channel of 75 m length and 30 m width with three mounds. The shape of the mounds is defined by the function $H(x, y) = \max(0, m_1, m_2, m_3)$, where

$$m_1 = 1 - 0.1\sqrt{(x-30)^2 + (y-22.5)^2},$$
$$m_2 = 1 - 0.1\sqrt{(x-30)^2 + (y-7.5)^2},$$
$$m_3 = 2.8 - 0.28\sqrt{(x-47.5)^2 + (y-15)^2}.$$

The topography has been discretized using a 60×150 quadrilateral mesh.

The upper and lower boundaries are assumed to be solid walls, while the right boundary represents an open wall and the left boundary simulates an inflow having the following form:

– From $t = 0$ to $t = 300$, the height is $h = 0.5$ and the velocity in the x direction is $u = 1.0$.
– From $t = 300$ to $t = 900$, we have $h = 1.0$ and $u = 1.0$.

Table 3
Two-dimensional accuracy test

Number of cells	Error h	Order h	Error q_1	Order q_1	Error q_2	Order q_2
25×25	1.52E−02	–	4.13E−02	–	9.10E−02	–
50×50	3.47E−03	2.13	8.33E−03	2.31	2.19E−02	2.05
100×100	5.45E−04	2.67	1.26E−03	2.72	3.50E−03	2.65
200×200	7.56E−05	2.85	1.77E−04	2.84	4.79E−04	2.87
400×400	9.79E−06	2.95	2.25E−05	2.97	6.28E−05	2.93

L^1 numerical errors and orders.

The results obtained at several times using the bi-hyperbolic HMRoe scheme with CFL number 0.9 are depicted in Fig. 13. It should be noticed that our results cannot be directly compared with those in [20], as we have not considered here turbulent viscosity nor friction terms. However, our results are consistent with the topography, also providing a good resolution of shocks and wet/dry transitions.

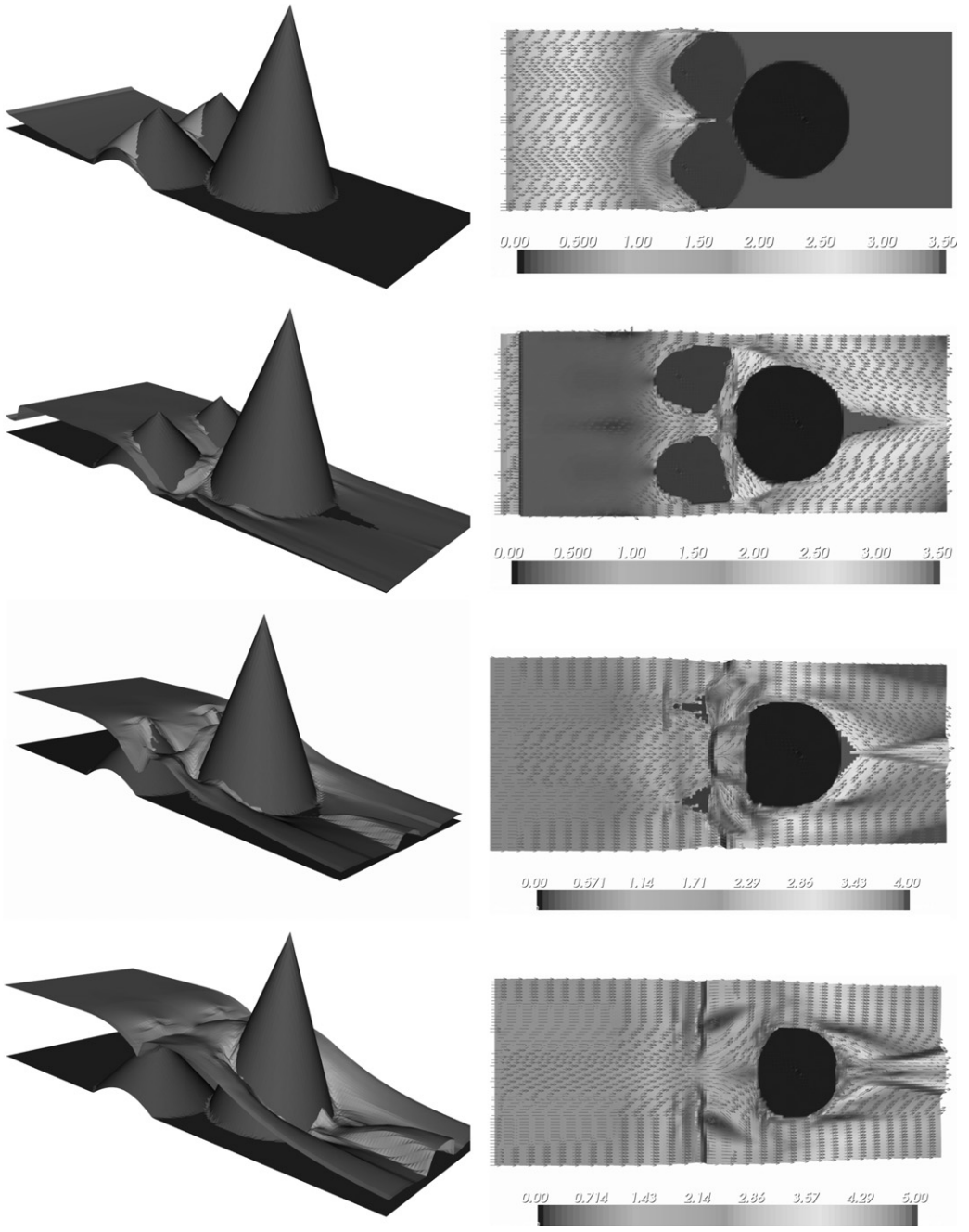

Fig. 13. Flooding on an open channel. From top to bottom: results obtained at times $t = 8$, 30, 300 and 900, using the bi-hyperbolic HMRoe scheme. Left: 3-D representation. Right: velocity fields.

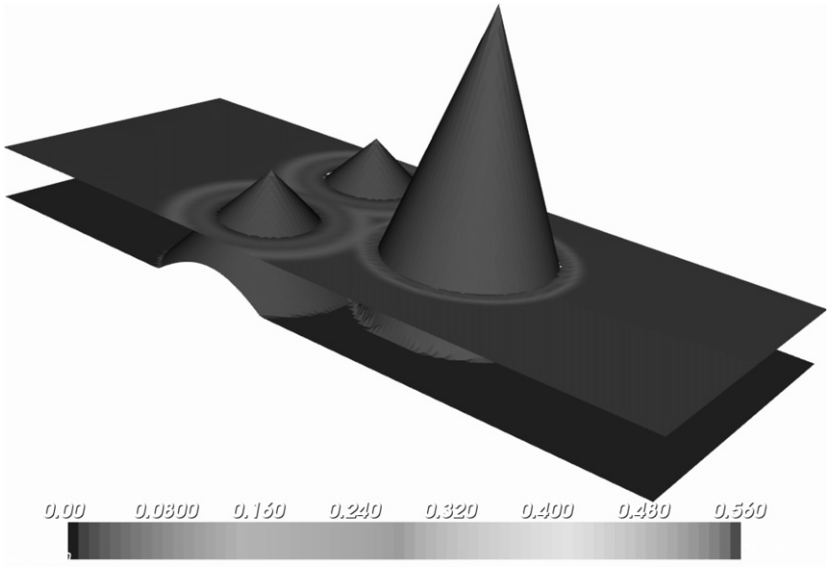

Fig. 14. Dambreak on a closed channel. 3-D view of the stationary state obtained with the bi-hyperbolic HMRoe scheme. The scale represents water height.

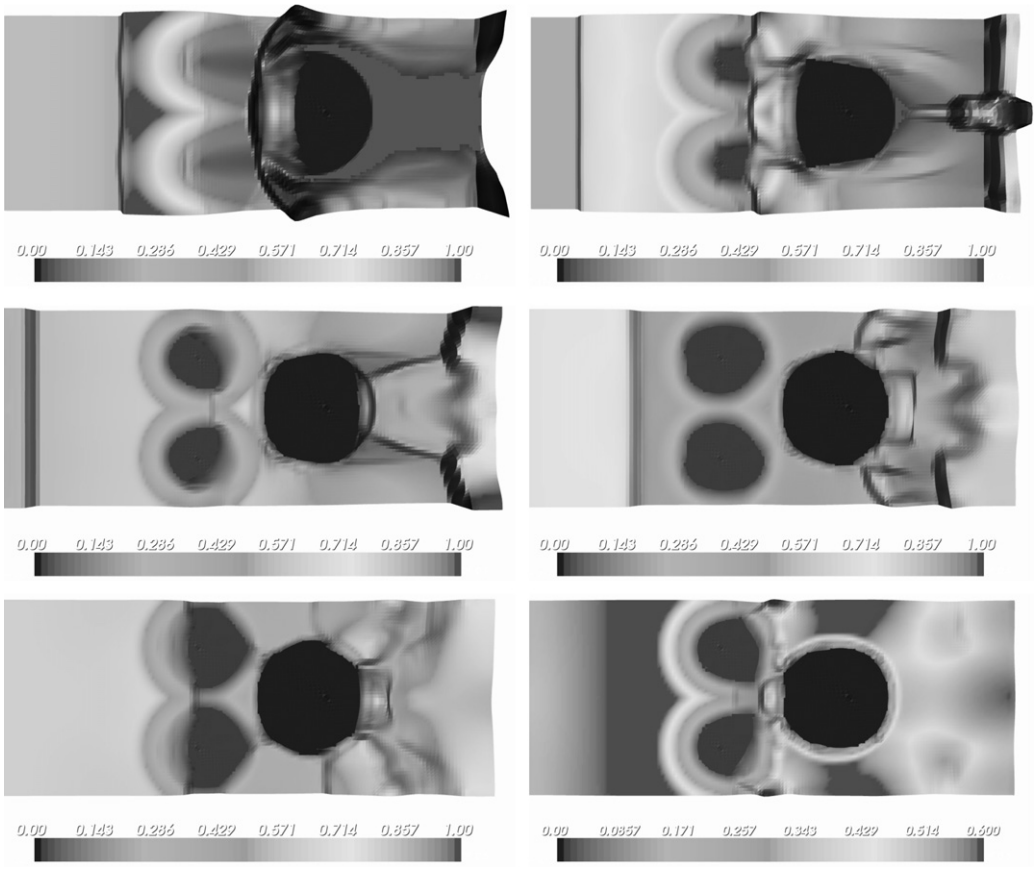

Fig. 15. Dambreak on an closed channel (upper view). From top to bottom and left to right: results obtained at times $t = 10$, 15, 20, 25, 30 and 40, using the bi-hyperbolic HMRoe scheme.

8.9. Dambreak on a closed channel

The same topography as in the previous test has been considered in [6] for simulating a dambreak. In this case all the boundaries are solid walls, so the water cannot leave the rectangular domain.

The dam is situated at $x = 16$ and contains $900\,\mathrm{m}^3$ of water. The scheme has been run until the stationary state is reached (Fig. 14), using a 60×150 mesh and CFL number 0.9. The results obtained at different times are shown in Fig. 15. As in the previous experiment, the results are physically consistent.

8.10. A two-dimensional oscillating lake

Consider the paraboloidal topography defined by the depth function

$$H(x,y) = h_0\left(1 - \frac{x^2+y^2}{a^2}\right), \quad (x,y) \in [-2,2] \times [-2,2],$$

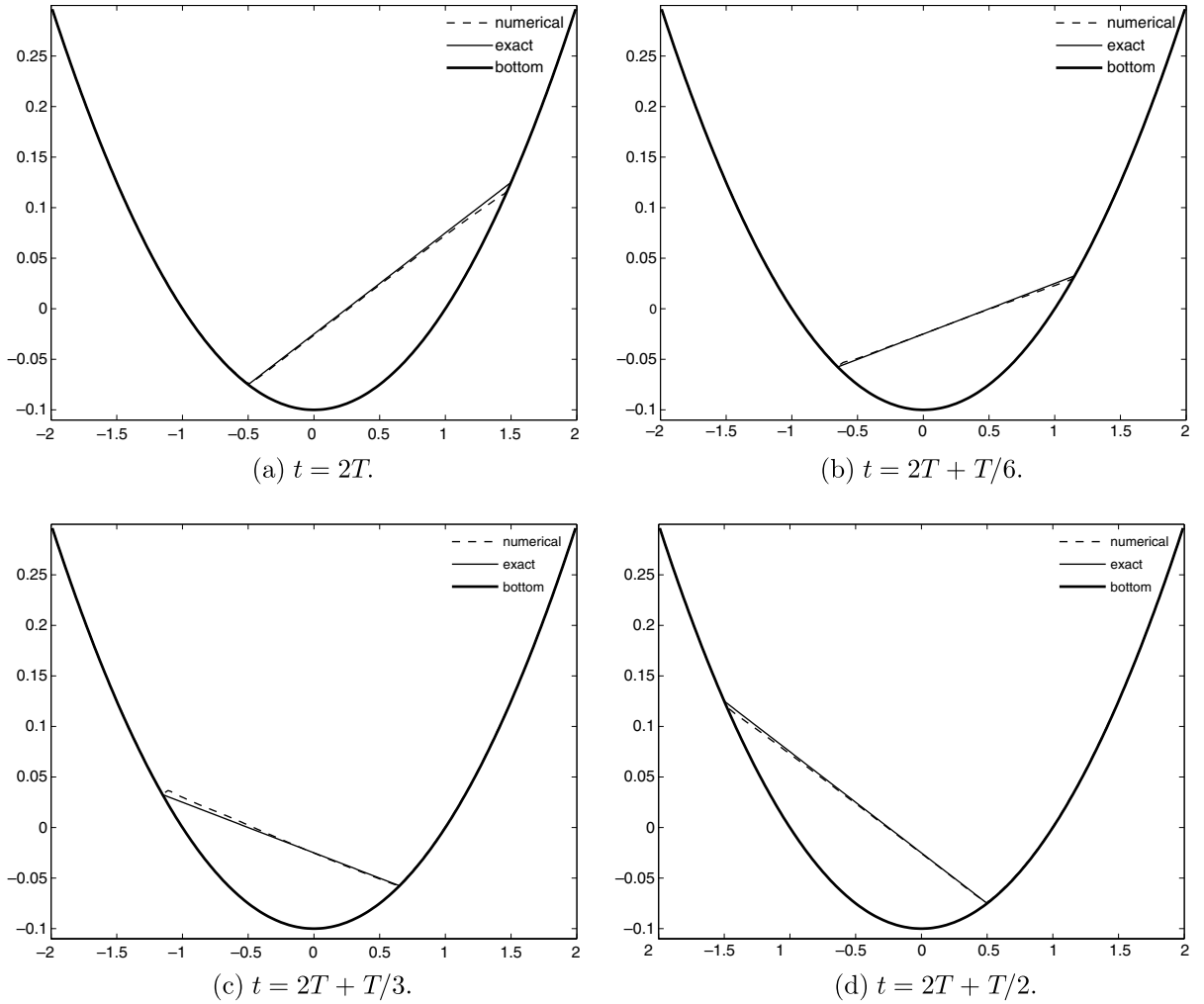

Fig. 16. 2-D oscillating lake: surface elevation vs. x-coordinate, for $y = 0$. Results obtained with the bi-hyperbolic HMRoe scheme.

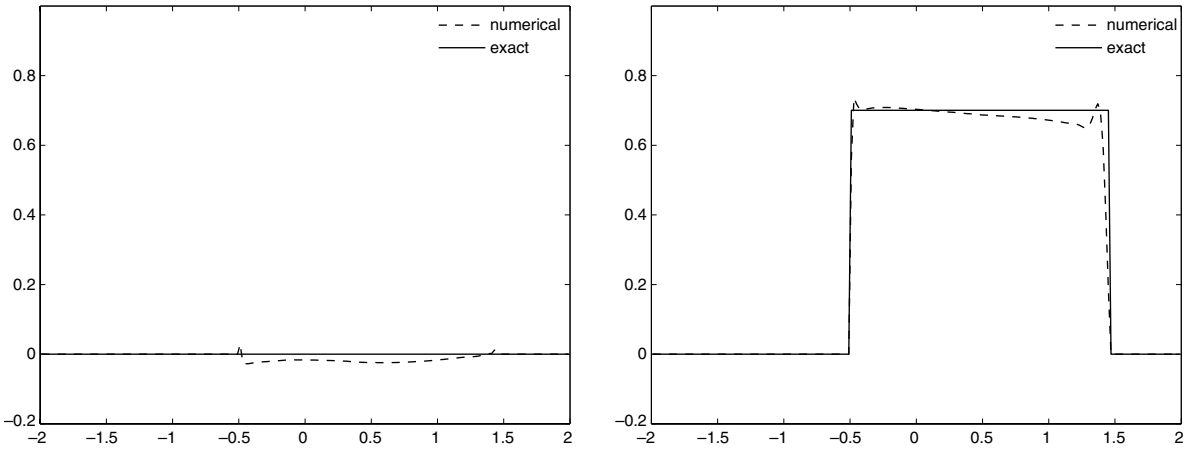

Fig. 17. 2-D oscillating lake: velocities at time $t = 2T$. Left: u. Right: v. Results obtained with the bi-hyperbolic HMRoe scheme.

together with the periodic analytical solution of the two-dimensional shallow water equations stated in [32]:

$$h(x,y,t) = \max\left(0, \frac{\sigma h_0}{a^2}(2x\cos(\omega t) + 2y\sin(\omega t) - \sigma) + H(x,y)\right),$$
$$u(x,y,t) = -\sigma\omega\sin(\omega t), \quad v(x,y,t) = \sigma\omega\cos(\omega t),$$

where u and v are the velocities in the x and y directions, and $\omega = \sqrt{2gh_0}/a$. The values $a = 1$, $\sigma = 0.5$ and $h_0 = 0.1$ have been considered for this test.

The computations have been performed using a quadrilateral mesh with $\Delta x = \Delta y = 0.02$ and CFL number 0.9. Comparisons between the numerical and the analytical free surfaces at different times are shown in Fig. 16, where T represents the oscillation period. Although a small distortion near the shorelines can be observed in some cases, they can be reduced using a finer spatial discretization. On the other hand, the planar form of the free surface is maintained throughout the computation.

To obtain accurate approximations of the velocity is a much more difficult issue. In Fig. 17 are shown comparisons for both the u and v velocities at time $t = 2T$. As it can be observed, the position of the wet/dry fronts have been accurately captured, despite the small perturbations appearing in the wet zone.

9. Concluding remarks

In this paper, a high-order finite volume scheme for solving shallow water equations in one and two space dimensions has been developed within a nonconservative framework. The scheme is able to handle wet/dry situations, and it is exactly well-balanced for water at rest solutions. It reaches third-order of accuracy on smooth wet regions, being only first-order accurate near shocks and wet/dry transitions. Imposing an adequate CFL restriction, the scheme preserves the positivity of the water height. Extensive numerical experiments have been performed in order to demonstrate the capabilities of the scheme.

Appendix. Positivity of the LHHR method

The positivity of the LHHR technique, which is a key point in Section 6, is proved in this section.

First of all, let us set the notation to be used in this section. Let $v(x)$ be the function to be reconstructed and consider the stencil $\{I_i: i = -1, 0, 1\}$, with $I_i = [x_{i-1/2}, x_{i+1/2}]$ and $x_{i\pm1/2} = x_i \pm \Delta x/2$. Define the lateral derivatives $d_L = (v_0 - v_{-1})/\Delta x$ and $d_R = (v_1 - v_0)/\Delta x$, where v_i is the average of $v(x)$ on the cell I_i.

We consider the version of the LHHR algorithm stated in [30]:

Let define $tol = \Delta x^2$,
if ($|d_L| \leqslant tol$) and ($|d_R| \leqslant tol$) **then**

$d_0 = 0 \quad \text{and} \quad \alpha = 0$

else

$$d_0 = (\operatorname{sgn}(d_L) + \operatorname{sgn}(d_R)) \frac{|d_L d_R|}{|d_L| + |d_R|}$$

if $|d_L| \leqslant |d_R|$ **then**

$$\alpha = 2\left(\sqrt{|d_0/d_L|} - 1\right)$$

else

$$\alpha = 2(1 - \sqrt{|d_0/d_R|})$$

end
end

Once d_0 and α have been defined, the reconstructing hyperbola on the cell I_0 is given by

$$r_0(x) = v_0 + d_0 \frac{\Delta x}{\alpha^2}\left(\log\left(\frac{2-\alpha}{2+\alpha}\right) - \frac{\alpha \Delta x}{\alpha(x - x_0) - \Delta x}\right).$$

Some useful remarks ([24], Lemma 2.2):

(1) $\alpha \in (-2(\sqrt{2}-1), 2(\sqrt{2}-1))$, independently of Δx.
(2) $r_0(x)$ is well-defined on I_0 and is monotone.
(3) When $\alpha = 0$, $r_0(x)$ reduces to the linear function

$$r_0(x) = v_0 + d_0(x - x_0). \tag{A.1}$$

Assume now that $v_i > 0$ for each $i = -1, 0, 1$; we are going to see that $r_0(x) > 0$ for every $x \in I_0$. We only need to consider the case in which $d_L d_R > 0$, as $r_0(x)$ reduces to the constant value v_0 in any other case.

We focus on the case $d_L > 0$ and $d_R > 0$ (the opposite case can be treated in an analogous way). We have that

$$d_0 = 2\frac{d_L d_R}{d_L + d_R}$$

and $r_0(x)$ is an increasing function. Three possibilities have to be considered:

(1) $d_L = d_R$.
(2) $d_L < d_R$.
(3) $d_L > d_R$.

In case (1) we have $\alpha = 0$, so $r_0(x)$ has the form (A.1). As $d_0 = d_L = d_R$, then

$$r_0(x_{-1/2}) = v_0 - d_0\frac{\Delta x}{2} = \frac{v_0 + v_{-1}}{2} > 0.$$

Using that $r_0(x)$ is increasing, we deduce that $r_0(x) > 0$ for $x \in I_0$.

Consider now case (2), in which $\alpha = 2(\sqrt{d_0/d_L} - 1) \in (0, 2(\sqrt{2}-1))$. The vertical asymptote of $r_0(x)$ is located in $(x_{1/2}, \infty)$, so $r_0(x)$ is well-defined on $I_{-1} \cup I_0$, where it is strictly increasing. It will more convenient to write $r_0(x)$ in the form

$$r_0(x) = a_0 + \frac{\lambda_0}{x - x_0 + c_0},$$

with

$$a_0 = v_0 + d_0 \frac{\Delta x}{\alpha^2} \log\left(\frac{2-\alpha}{2+\alpha}\right), \quad c_0 = -\frac{\Delta x}{\alpha}, \quad \lambda_0 = -d_0 \left(\frac{\Delta x}{\alpha}\right)^2.$$

Clearly, in order to prove the positivity of $r_0(x)$ on I_0 it is sufficient to see that $r_0(x_{-1/2}) > 0$, or, equivalently,

$$a_0 + \lambda_0 (c_0 - \Delta x/2)^{-1} > 0.$$

From the definitions of c_0 and λ_0, we have:

$$\lambda_0 (c_0 - \Delta x/2)^{-1} = 2 d_0 \frac{\Delta x}{\alpha(2+\alpha)}. \tag{A.2}$$

On the other hand, we have that

$$a_0 > v_0 - 2 d_0 \frac{\Delta x}{\alpha(2+\alpha)} - 4 d_0 \frac{\Delta x}{(2+\alpha)^2},$$

that follows from the definition of a_0 and the trivial inequality $\log\left(\frac{2-\alpha}{2+\alpha}\right) > -\frac{2\alpha}{2+\alpha} - \left(\frac{2\alpha}{2+\alpha}\right)^2$ for $\alpha \in (0, 2(\sqrt{2}-1))$. Now, using the definition of α, the above expression can be written as

$$a_0 > v_0 - d_{\mathrm{L}} \Delta x - 2 \frac{d_0 \Delta x}{\alpha(\alpha+2)}. \tag{A.3}$$

Combining (A.2) and (A.3), we deduce:

$$a_0 + \lambda_0 (c_0 - \Delta x/2)^{-1} > v_0 - d_{\mathrm{L}} \Delta x = v_{-1} > 0,$$

as desired.

Finally, case (3) can be analyzed in a similar way as case (2).

References

[1] R. Artebrandt, H.J. Schroll, Limiter-free third order logarithmic reconstruction, SIAM J. Sci. Comput. 28 (2006) 359–381.

[2] E. Audusse, F. Bouchut, M.-O. Bristeau, R. Klein, B. Perthame, A fast and stable well-balanced scheme with hydrostatic projection for shallow water flows, SIAM J. Sci. Comput. 25 (2004) 2050–2065.

[3] D.S. Bale, R.J. LeVeque, S. Mitran, J.A. Rossmanith, A wave propagation method for conservation laws and balance laws with spatially varying flux functions, SIAM J. Sci. Comput. 24 (2002) 955–978.

[4] A. Bermúdez, M.E. Vázquez, Upwind methods for hyperbolic conservation laws with source terms, Comput. Fluids 23 (1994) 1049–1971.

[5] F. Bouchut, Nonlinear Stability of Finite Volume Methods for Hyperbolic Conservation Laws and Well-Balanced Schemes for Sources, Birkäuser, 2004.

[6] P. Brufau, M.E. Vázquez, P. García, A numerical model for the flooding and drying of irregular domains, Int. J. Numer. Meth. Fluids 39 (2002) 247–275.

[7] T. Buffard, T. Gallouët, J.-M. Hérard, A sequel to a rough Godunov scheme: application to real gases, Comput. Fluids 29 (2000) 813–847.

[8] M. Castro, J.M. Gallardo, C. Parés, High order finite volume schemes based on reconstruction of states for solving hyperbolic systems with nonconservative products. Applications to shallow water systems, Math. Comput. 75 (2006) 1103–1134.

[9] M.J. Castro, J.M. González, C. Parés, Numerical treatment of wet/dry fronts in shallow flows with a modified Roe scheme, Math. Mod. Meth. Appl. Sci. 16 (2006).

[10] M.J. Castro, A. Ferreiro, J.A. García, J.M. González, J. Macías, C. Parés, M.E. Vázquez-Cendón, On the numerical treatment of wet/dry fronts in shallow flows: application to one-layer and two-layers systems, Math. Comput. Mod. 42 (2005) 419–439.

[11] G. Dal Maso, Ph. LeFloch, F. Murat, Definition and weak stability of nonconservative products, J. Math. Pures Appl. 74 (1995) 483–548.

[12] F. Dubois, Partial Riemann problems, boundary conditions and gas dynamics, in: Absorbing Boundaries and Layers, Domain Decomposition Methods, Nova Sci. Publ., Huntington, NY, 2001, pp. 16–77.

[13] T. Gallouët, J.-M. Hérard, N. Seguin, Some approximate Godunov schemes to compute shallow-water equations with topography, Comput. Fluids 32 (2003) 479–513.

[14] L. Gosse, A well-balanced flux-vector splitting scheme designed for hyperbolic systems of conservation laws with source terms, Comput. Math. Appl. 39 (2000) 135–159.
[15] S. Gottlieb, C.-W. Shu, Total variation diminishing Runge–Kutta schemes, Math. Comput. 67 (1998) 73–85.
[16] J.M. Greenberg, A.Y. LeRoux, A well-balanced scheme for the numerical processing of source terms in hyperbolic equations, SIAM J. Numer. Anal. 33 (1996) 1–16.
[17] A. Harten, J.M. Hyman, Self-adjusting grid methods for one-dimensional hyperbolic conservation laws, J. Comput. Phys. 50 (1983) 235–269.
[18] A. Harten, B. Engquist, S. Osher, S. Chakravarthy, Uniformly high order essentially non-oscillatory schemes III, J. Comput. Phys. 71 (1987) 231–303.
[19] G. Jiang, C.-W. Shu, Efficient implementation of weighted ENO schemes, J. Comput. Phys. 126 (1996) 202–228.
[20] M. Kawahara, T. Umetsu, Finite element method for moving boundary problems in river flow, Int. J. Numer. Meth. Fluids 6 (1986) 365–386.
[21] P.G. LeFloch, Shock waves for nonlinear hyperbolic systems in nonconservative form, Institute for Math. and its Appl., Minneapolis, Preprint 593, 1989.
[22] R.J. LeVeque, Balancing source terms and flux gradients in high-resolution Godunov methods: the quasi-steady wave-propagation algorithm, J. Comput. Phys. 146 (1998) 346–365.
[23] X.D. Liu, S. Osher, T. Chan, Weighted essentially nonoscillatory schemes, J. Comput. Phys. 115 (1994) 200–212.
[24] A. Marquina, Local piecewise hyperbolic reconstructions for nonlinear scalar conservation laws, SIAM J. Sci. Comput. 15 (1994) 892–915.
[25] C.-D. Munz, A tracking method for gas flow into vacuum based on the vacuum Riemann problem, Math. Methods Appl. Sci. 17 (1994) 597–612.
[26] S. Noelle, N. Pankratz, G. Puppo, J.R. Natvig, Well-balanced finite volume schemes of arbitrary order of accuracy for shallow water flows, J. Comput. Phys. 213 (2006) 474–499.
[27] C. Parés, M. Castro, On the well-balanced property of Roe's method for nonconservative hyperbolic systems. Applications to shallow water systems, ESAIM: M2AN 38 (2004) 821–852.
[28] P.L. Roe, Approximate Riemann solvers, parameter vectors and difference schemes, J. Comput. Phys. 43 (1981) 357–371.
[29] H.J. Schroll, F. Svensson, A bi-hyperbolic finite volume method on quadrilateral meshes, J. Sci. Comput. 26 (2006) 237–260.
[30] S. Serna, A class of extended limiters applied to piecewise hyperbolic method, SIAM J. Sci. Comput. 28 (2006) 123–140.
[31] C.-W. Shu, S. Osher, Efficient implementation of essentially non-oscillatory shock capturing schemes, J. Comput. Phys. 77 (1998) 439–471.
[32] W.C. Thacker, Some exact solutions to the nonlinear shallow-water wave equations, J. Fluid Mech. 107 (1981) 499–508.
[33] E.F. Toro, Shock-Capturing Methods for Free-Surface Shallow Flows, John Wiley & Sons, 2001.
[34] I. Toumi, A weak formulation of Roe's approximate Riemann solver, J. Comput. Phys. 102 (1992) 360–373.
[35] S. Vukovic, L. Sopta, ENO and WENO schemes with the exact conservation property for one-dimensional shallow water equations, J. Comput. Phys. 179 (2002) 593–621.
[36] Y. Xing, C.-W. Shu, High order finite difference WENO schemes with the exact conservation property for the shallow water equations, J. Comput. Phys. 208 (2005) 206–227.
[37] Y. Xing, C.-W. Shu, High order well-balanced finite volume WENO schemes and discontinuous Galerkin methods for a class of hyperbolic systems with source terms, J. Comput. Phys. 214 (2006) 567–598.